Eastern Kentucky University
Encompass

Online Theses and Dissertations

Student Scholarship

January 2016

Toward the Synthesis and Characterization of Pb-Doped ZnS Nanocrystals for Solar Energy Applications

Allison Durr
Eastern Kentucky University

Follow this and additional works at: https://encompass.eku.edu/etd

Part of the Biochemical and Biomolecular Engineering Commons

TOWARD THE SYNTHESIS AND CHARACTERIZATION OF

Pb-DOPED ZnS NANOCRYSTALS FOR SOLAR ENERGY APPLICATIONS

By

Allison Laurie Durr

Thesis Approved:

_____
Chair, Advisory Committee

_____
Member, Advisory Committee

Pei Gao

_____
Member, Advisory Committee

_____
Dean, Graduate School

STATEMENT OF PERMISSION TO USE

In presenting this thesis, in partial fulfillment of the requirements for a Master's degree at Eastern Kentucky University, I agree that the Library shall make it available to borrowers under rules of the Library. Brief quotations from this thesis are allowable without special permission, provided that accurate acknowledgment of the source is made. Permission for extensive quotation from or reproduction of this thesis may be granted by my major professor, or in [his/her] absence, by the Head of Interlibrary Services when, in the opinion of either, the proposed use of the material is for scholarly purposes. Any copying or use of the material in this thesis for financial gain shall not be allowed without my written permission.

Signature _____

Date ___05/23/16_____

TOWARD THE SYNTHESIS AND CHARACTERIZATION OF

Pb-DOPED ZnS NANOCRYSTALS FOR SOLAR ENERGY APPLICATIONS

By

Allison Laurie Durr

Bachelor of Arts

Eastern Kentucky University

Richmond, Kentucky

2014

Submitted to the Faculty of the Graduate School of

Eastern Kentucky University

in partial fulfillment of the requirements

for the degree of

MASTER OF SCIENCE

August, 2016

DEDICATION

This thesis is dedicated to my wonderful and supportive fiancé, Ross Morgan. Without his constant reassurance and encouragement this work could not have been completed. Also, to my loving parents, David and Laurie Durr, who have always believed in me and supported my enthusiasm and passion for the chemistry field. To all of my family and friends, both new and old, who have remained optimistic and positive about this thesis project and my future career, thank you for the amazing support and kind thoughts throughout this process. Lastly, to my mentor Dr. Judy Jenkins, without whom I would not be the person nor the scientist I am today.

ACKNOWLEDGMENTS

ABSTRACT

Efficient and affordable energy conversion and energy storage technologies are required to meet society's increasing demands. Semiconductor nanocrystals are particularly attractive materials for solar energy conversion applications, as their tunable optoelectronic properties can be manipulated to both optimize the absorbance of solar photons and to afford desirable electronic properties. Further tunability of binary semiconductor nanocrystal systems can be realized through substitutional doping. However, doping can be difficult, as the dopants can cause significant lattice strain in the host crystals. Lead-doped ZnS nanocrystals are one promising material for the conversion of solar photons into storable fuels such as hydrogen gas. The ZnS conduction band is sufficiently high in energy to reduce protons, and the lead dopants are hypothesized to add filled states in the ZnS band gap, thereby extending the absorbance of the crystals into the visible region. This work details progress towards controllable doping of ZnS nanocrystals with lead cations using modified hot injection procedures. Preliminary results suggest that the temperature of the ZnS reaction matrix, the temperature of the Pb reaction flask, and the mole ratio between Pb and Zn can be used to afford various mixtures of ZnS and PbS nanocrystals with various sizes and optical properties. Spectroscopic data demonstrates synthesis-dependent optical and electronic properties, and high resolution transmission electron micrographs provide structural information.

TABLE OF CONTENTS

LIST OF TABLES

LIST OF FIGURES

LIST OF ABBREVIATIONS

Greenhouse Gases .... GHGs

Infrared .... IR

Carbon Dioxide.. CO_2

Hydrogen Gas.. H_2 *(g)*

Ultraviolet-Visible ....UV-Vis

Conduction Band... CB

Valance Band..VB

Nanocrystal ....NC

Lead Doped Zinc Sulfide...Pb-doped ZnS

Zinc Sulfide ....ZnS

Lead Sulfide .... PbS

Infrared .... IR

Transmission Electron Microscopy .... TEM

Electron-Dispersive X-ray Spectroscopy .... EDS

Lead Oleate Complex .... $Pb(OA)_2$

Bis(trimethylsilyl)sulfide .... TMS

Nuclear Magnetic Resonance .... NMR

Photoluminescence...PL

Rate of Formation .... k_f

Rate of Nucleation .... k_n

Rate of Growth.. k_g

Rate of Diffusion .... k_d

Gibbs Free Energy ....ΔG

CHAPTER 1

THE BIG PICTURE

1.1 Introduction

The energy needs of the world continue to grow as the world becomes more and more industrialized. In 2007 the average consumption of energy was 16.2 terrawatts.[1] That means in 2007 alone, the world would have needed to burn 1.701×10^{10} pounds of coal to produce the amount of energy consumed, if coal was the only form of energy the world had.[2] The burning of this much coal or other fossil fuels releases large amounts of greenhouse gasses (GHGs) into the atmosphere, which can have damaging effects. The global energy need is predicted to triple by 2100 due to a rise in population.[1] To make the problem more complicated, fuel sources are often logistically difficult to retrieve or located in politically volatile regions. Thus, the world must develop alternative methods for the collection and storage of energy.

The atmosphere contains three main GHGs: carbon dioxide, nitrous oxide, and methane.[3] These GHGs absorb infrared (IR) radiation that that is reflected off of the Earth's surface, other gases, or clouds. A depiction of this can be seen in **Figure 1.1**. This causes the excited molecules to vibrate, emitting the energy in all directions. Some of the radiation is emitted towards Earth's surface, thereby heating of the surface which then heat the adjacent air mass.[3] In fact, average air temperature over land has

increased by 0.27 °C/decade since 1979.[3] Carbon dioxide and methane are two of the

largest contributors of the GHGs. Carbon dioxide has four vibrational modes, two of

which, bend (672.6 cm^{-1}) and asymmetric stretch (2396.3 cm^{-1}), absorb IR radiation and

cause the molecule to vibrate.[4] Methane also has four vibrational mode, two of which,

wag (1367.4 cm^{-1}) and asymmetric stretch (3156.8 cm^{-1}) absorb IR light and cause the

molecule to vibrate and release energy in the form of heat.[4]
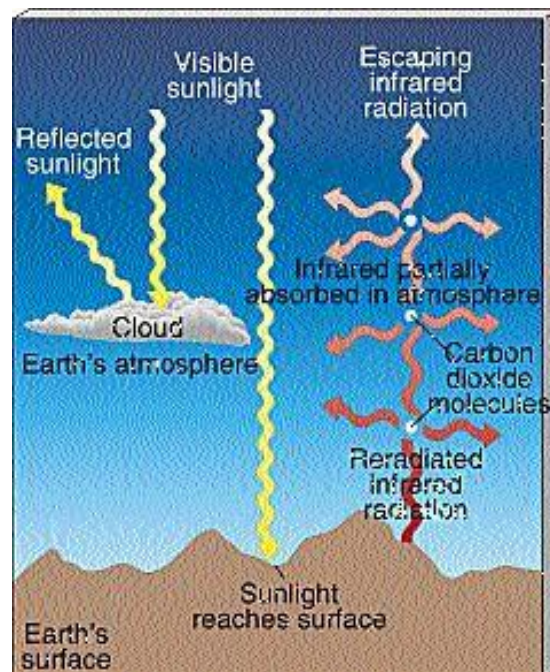
Figure 1.1 The greenhouse effect caused by visible light hitting the Earth's surface and

reflecting off of it to hit carbon dioxide and other GHGs causing the GHGs to vibrate and

release energy in the form of IR light. Source: Corey, P.; Reeves, A. The Earth: Our

Homespace   http://staff.on.br/jlkm/astron2e/AT_MEDIA/CH07/CHAP07AT.HTM

(accessed Feb 15, 2016).

2

GHG emission can result from natural processes, such as a volcanic eruption, as well as human processes, such as factories and farming. An increase in GHGs has been seen throughout the industrial period. GHGs like carbon dioxide (CO_2) are produced through the burning of fossil fuels. Once carbon dioxide is present in the atmosphere it becomes extremely difficult to remove it; the lifetime of carbon dioxide in Earth's atmosphere is 50-100 years.[5] The decomposition of oceanic carbon dioxide occurs through dissolved CO_2 and the dissolution of calcium and magnesium carbonate. It may take up to 7,000 years for CO_2 to be removed from the oceans.[3] The rise in concentration of GHGs like carbon dioxide and the corresponding increases in atmospheric and ocean temperatures are leading to increases in snow and ice melting, increases acidification of the world's oceans, and a rise in overall sea levels. This can have negative effects, because rising sea levels will decrease land masses and thus decrease animal and human habitats and crop growing area. Acidification of the oceans will lead to marine animals' death which will decrease the amount that humans can consume.

Due to the increase in demand for energy, the difficulty to reach some energy sources, and the release of GHG that cause rapid and potentially dangerous climate change, the development of a new energy supply system must be a priority. The energy supply system must be abundant, efficient, cost effective, and environmentally friendly. Alternative energy sources such as, bioenergy, wind energy, nuclear energy, and solar energy, are in development, as each of these sources has strengths and weaknesses.

Bioenergy results from the burning of biomass, such as a wood and crops, for the production of electrical energy from heat (similar to the ways in which coal is burned for energy). Wind energy results from wind powered turbines that transform the energy created from the motion of the turbines into electrical energy for human use. Nuclear energy results from the fission of nuclei that is converted into electrical energy. Lastly, solar energy is the energy that results from the absorption of solar photons (aka sunlight) and its excitation of electrons to form a storable energy. Solar energy conversion and storage is the motivation for the research described here.

Solar energy is an attractive energy source because of the sheer amount of energy available in sunlight. If the world collected all of the suns photons that hit Earth's surface in just one hour and then converted those photons to electrons with 100% efficiency, the entire planet could be powered for one year.[6] Thus, collecting a smaller portion of solar photons regularly could provide more than enough electricity to meet our world's growing needs. Unfortunately, the technology has not been developed yet that would allow for the collection of all of the solar photons that hit Earth's surface, nor the 100% conversion of photons to electrons. In fact, today's commercially available solar cells have the capacity to convert solar photons to electrons with only 11-15% efficiency.[7] Ongoing research will yield increasingly efficient solar cells, but higher efficiency alone will not solve all the energy problems.

The key factor that limits the impact of solar electricity in addressing growing energy needs is that electricity generated from sunlight is not available when the sun is

not shining. If the energy is not used shortly after collection and conversion to electricity, this energy is lost. Thus, it is absolutely critical that storage methods for solar energy are developed. Once an effective storage method for this energy is found, the energy can be generated locally, stored until needed, and easily transported without the need for preexisting electrical grids.[1] One possible method for the storage of solar energy is to convert the solar energy into chemical energy. For instance, a photocatalyst could absorb solar photons to generate high energy electrons, which can be used to form chemical bonds in a storable fuel such as hydrogen gas (H_2 *(g)*), shown in **Figure 1.2**. The research described here focusses on the synthesis of a photocatalyst for solar hydrogen generation.
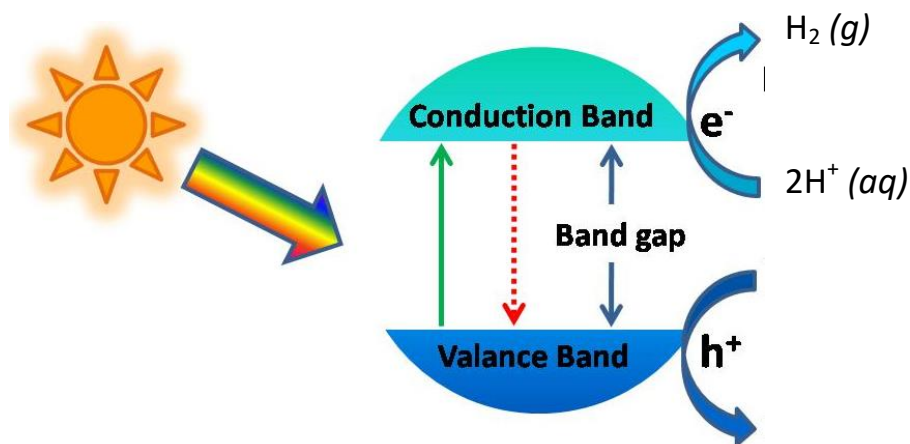
Figure 1.2: A generic diagram depicting photocatalytic H_2 (g) generation. H^+ is indicative of a proton. This excess proton can be found in acidic water (H_3O^+). When two protons get reduced next to each other or in rapid succession then they can form H_2 *(g)*. Source: Kamat, P. Photocatalysis https://www3.nd.edu/~kamatlab/research_photo catalysis.html (accessed Mar 1, 2016).

The reaction for the formation of hydrogen gas (Eqn. 1) consists of two hydrogen ions reacting with two electrons to create hydrogen gas. The two hydrogen ions come from the water. The electrons come from the photocatalyst. Once a photocatalyst is synthesized, it will be placed in water with sacrificial electron donors, in this case sulfides and sulfoxides. These sacrificial electron donors are also used to prevent the oxidation of the photocatalyst as depicted in **Figure 1.3**.[9] While our photocatalyst is designed specifically for hydrogen reduction, it is similar in operation to water-splitting photocatalysts, where the valance band (VB) is lower in energy than the energy than the standard reduction potential for the conversion of hydroxide ions to oxygen gas, so it is possible to produce oxygen gas and hydrogen gas simultaneously (Eqn. 2). In the case of the photocatalyst described in this thesis, production of excess oxygen would oxidatively degrade our photocatalyst. For our photocatalyst the VB is higher in energy that the reduction potential of hydroxide ions to oxygen gas so instead our photocatalyst has the potential to be oxidized instead of producing oxygen gas, hence the need for the sacrificial reagents during operation.

$2H^+ (aq) + 2e^- \rightarrow H_2 (g)$ (1)

$2\ H_2O(l) + 2e^- \rightarrow H_2(g) + 2\ OH^-(aq)$ (2a)

$4\ OH^-(aq) \rightarrow O_2(g) + 2\ H_2O(l) + 4\ e^-$ (2b)
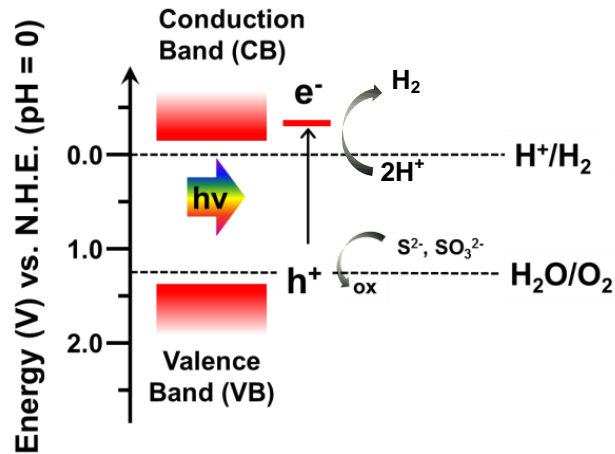
Figure 1.3: The VB and CB of an ideal photocatalyst. Note the CB is higher than the energy to convert H^+ to H_2.

The excess electrons from the donors replenish the electrons in the photocatalyst. The energy needed to supply the excitement of an electron as well as the electron transfers to form chemical bonds is provided by the solar photons.

Once hydrogen gas is generated, it can be used in many different platforms including electricity generation, powering the transportation industry, or powering residential, commercial, or industrial facilities. Plus, after hydrogen gas is used in these ways, the byproduct of its consumption is water, making hydrogen gas a clean and renewable energy source. The world may be able to run on a hydrogen economy as displayed in **Figure 1.4**.[10]
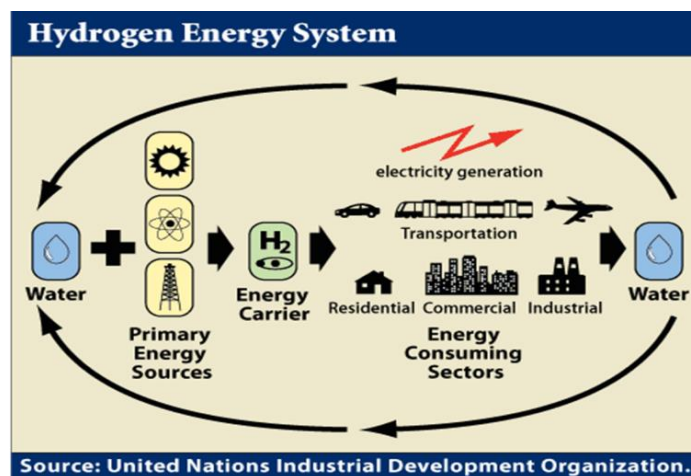
Figure 1.4: The hydrogen economy system. Source: United Nations Industrial Development Organization, http://www.window.state.tx.us/specialrpt/energy/renewable/h2.php (accessed Mar. 1, 2016).

1.2 Photocatalyst Design Criteria

The research described here focusses on the synthesis of a photocatalyst for use in the generation of hydrogen gas using sunlight. A good photocatalyst will need to meet at least four criteria in order to be considered a viable candidate for the conversion of solar energy into storable hydrogen gas.

1. *The photocatalyst must be able to absorb solar photons.* The majority (71.6%) of solar photons emitted from the sun are in the 400-800 nm range.[11] This is shown in **Figure 1.5**. The absorbance of a photocatalyst can be monitored with ultraviolet-visible (UV-Vis) spectroscopy.

8
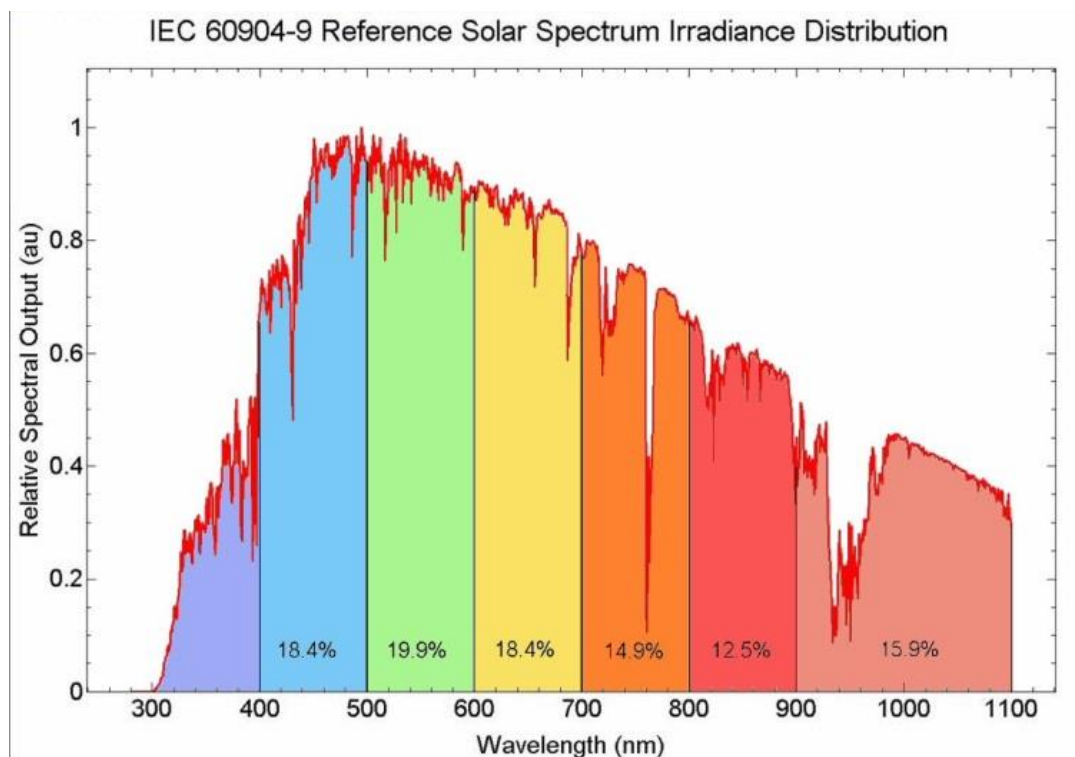
Figure 1.5: The relative spectral output of the sun at certain wavelengths of light. Source: International Standard - Switzerland http://www.iec.ch/ (accessed Feb 1, 2016).

2. *The photocatalyst must have sufficient conduction band energy for the reduction of H$^+$ (aq) to H$_2$ (g).* **Figure 1.3** shows a depiction of a conduction band (CB) and valance band (VB). In order to be a good photocatalyst for hydrogen generation the energy of the CB must be above the reduction potential of H$^+$ *(aq)* to H$_2$ *(g)*. If the conduction band is above the reduction potential of H$_2$ *(g)* and the photocatalyst absorbs solar photons, then the solar photons will excite electrons from the VB to the CB, and then those electrons would be of sufficient energy to reduce H$^+$ *(aq)* to H$_2$ *(g)*.

9

3. *The photocatalyst must be comprised of a robust material with a high surface area.*

    The photocatalyst used must be made up of a compound that will be able to reduce

    many H^+ *(aq)* ions to H_2 *(g)*. If the material only reduced one ion then degrades it

    would not be a cost effective photocatalyst. The photocatalyst must also be able to

    work for long periods of time in order to be cost effective. This means that the

    photocatalyst may undergo little to no photocorrosion when under constant

    exposure to light.[12] The ideal photocatalyst has a high surface area because

    hydrogen ions must interact with the surface of the NCs for the necessary electron

    transfer reactions to occur. The most used shape for photocatalyst is a spherical

    nanocrystal (NC). Spherical NCs have a high ratio of surface atoms to total atoms,

    which provides many reaction sites for the reduction of H^+ *(aq)* to H_2 *(g)* to occur.

    Thus the shape minimizes the number of atoms in the bulk of the spherical NC while

    maximizing the number of available catalytic sites on the surface of the NC. With a

    high surface area it is possible to more easily control the rates at which these

    hydrogen gas generation reactions occur. If there is a large surface area the odds of

    a photogenerated electron coming into contact with a hydrogen ion is greatly

    increased. If the surface area is lowered then current densities are increased

    because more electrons would need to be produced in the bulk to increase the

    likelihood of an electron/hydrogen ion encounter. Lower surface area also leads to

    electrons losing energy over time as they wait for their encounter with a hydrogen

    ion. To counter this higher energy electrons, and thus high overpotentials, would be

needed to keep the electrons at a high enough energy. The high surface atoms to volume ratio of a spherical NC allows for the water redox reaction to occur at low current densities and low overpotenials. This simply means that the increased surface area better matches the photocurrents with the slow water splitting reaction.[12] The need for fast, highly reactive photocatalyst is reduced because of the large surface area.

4. *The photocatalyst must be made from cheap, earth abundant materials*. For the photocatalyst is to be economically viable, it must be cost effective to make for mass production in order to compete with the costs of fossil fuels. The photocatalyst developed in this thesis is made from both cheap, and earth abundant materials.

1.3 Lead-Doped Zinc Sulfide Nanocrystaline Photocatalysts

While there are different kinds of photocatalysts, this thesis will focus on doped semiconducting photocatalysts for the reduction of hydrogen ions to hydrogen gas via sunlight. As will be discussed in detail below, we hypothesize that a photocatalyst made from a combination of lead, zinc, and sulfur will be a good photocatalyst for hydrogen gas generation—specifically zinc sulfide nanocrystals doped with lead ions. If the lead is doped into the zinc sulfide structure, the resulting lead doped zinc sulfide (Pb-doped ZnS) should absorb the appropriate wavelengths of solar photons, have a CB above the

reduction potential of H_2 *(aq)*, be robust with a high surface area, and be made of cheap, earth abundant material.

As shown in **Figure 1.6**, zinc sulfide (ZnS) has a CB sufficient for the reduction of H^+ *(aq)* to H_2 *(g)*, because its CB is above the energy required for this reduction. However, the gap between the VB and CB, often referred to as the band gap, is extremely large. It takes very high energy photons to excite electrons from the VB to the CB. ZnS only absorbs photons that are ~ 335 nm and higher in energy. Thus, ZnS by itself is not a good photocatalyst for H_2 *(g)* production, as it does not fall in the previously stated 400-800 nm range. PbS can absorb nearly the entire UV-vis spectrum as shown by its small bandgap in **Figure 1.6**. The CB of lead sulfide (PbS) is just above the energy required for the reduction of H^+ *(aq)*. However, practically speaking, a slight overpotential is required for efficient production of H_2 *(g)*. Thus, neither ZnS nor PbS alone is an ideal photocatalyst for solar hydrogen generation.
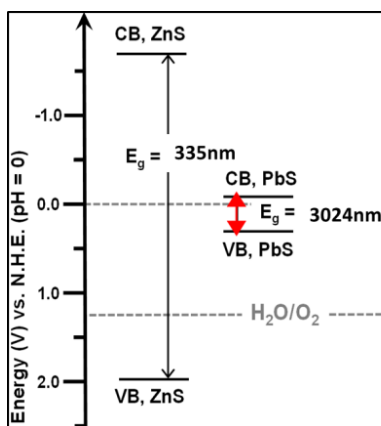
Figure 1.6: Energy level diagram for ZnS and PbS. Source: Tsuji, I.; Kudo, A. *J. Photochem. Photobiol. A Chem.* **2003**, *156*, 249–252.

The NC structures are different as well. ZnS most commonly exists in a wurzite crystal structure, where the zinc and sulfur are in tetrahedral environments. The PbS exists in rock salt, cubic structure, where lead and sulfur are each in an octahedral environments.

Pb-doped ZnS NCs is a system that has not been controllably synthesized. However, bulk Pb-doped ZnS has been generated by a group from the University of Tokyo.[13] The optical and electronic properties of their materials are shown in **Figure 1.7**.[13] Lead doping is thought to introduce filled Pb 6s states into the ZnS bandgap such that more solar photons can be absorbed while the ZnS CB energy is maintained. Tsuji et al. found that bulk Pb-doped ZnS absorbed photons at around 540 nm. The doped NC would most likely be a slightly distorted the wurzite structure, with one Zn atom being replaced by one Pb atom due to the Pb atom being much larger than the Zn atoms.
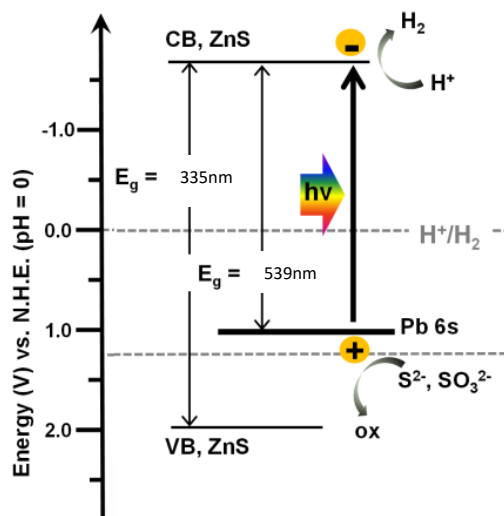
Figure 1.7: The measured VB and CB configuration for Pb-doped ZnS bulk material.

Source: Tsuji, I.; Kudo, A. *J. Photochem. Photobiol. A Chem.* **2003**, *156*, 249–252.

It is important to note that NCs, regardless of crystal structure and doping, are composed of surface atoms and bulk atoms. The bulk atoms are located in the center of the NC and bulk atoms (X) are attached to by other atoms (Y) that are all identical (ex. XY_4). Since these bulk atoms exist in one conformation, fully coordinated by identical elements, bands of electronic states form, and the difference between the filled states and empty states is referred to as the band gap and corresponds to an electronic transition between the bulk VB and CB. The surface atoms are any atoms that exist on the surface of a NC. These surface atoms (A) can exist in many different states due to the high number of possible combinations of atoms (B and C) that can exist on the surface (ex. AB_3C, AB_2C_2, ABC_3). The atoms may not be fully coordinated, and are therefore highly reactive. Additionally, the atoms may be coordinated to dissimilar atoms—partially coordinated by ligands and partially coordinated by bulk atoms. Since there are many possible bonding combinations for surface atoms, discreet energy states corresponding to the various combinations exist over a broad energy range between the bulk CB and VB. These energy states are referred to as midgap states, surface states, or trap states, and these states may be occupied (by electrons) or unoccupied.

Due to these different types of coordination in NC atoms there are different types of doping, bulk doping and surface doping. In bulk doping, the doped atoms exist in bulk feature of NC. Bulk dopants may substitutionally replace other bulk atoms, and these dopants can cause distortions in the crystal structure due to differences in size,

coordination number, etc. In surface doping, the doped atoms are only incorporated onto the surface of the NC. It is unclear which type of doping would afford a more stable or powerful photocatalyst, but the doping that does occur should be a very low doping density, perhaps only 1-2 atoms per NC. This low doping density discourages the formation of discrete PbS sections within the overall ZnS structure. Both bulk and surface doping are expected to introduce filled mid-gap states that are thought to correspond with the energy of the Pb 6s electrons, as shown in **Figure 1.7**.

If realized, the doping of Pb into a ZnS structure will result in NCs that absorb solar photons to excite electrons from the filled Pb orbitals to the ZnS CB such that reduction of H^+ *(aq)* to H_2 *(g)* can occur efficiently. The resulting photocatalyst will be made of a robust, cheap, and earth abundant material while also being able to absorb a large amount of solar photons. The material will also have a larger surface area for the catalytic sites so that this photocatalyst will be able to compete with the currently available fuel systems and will reduce the amount of GHGs released into the atmosphere.

1.4 Thesis Overview

This thesis will focus on the synthesis of Pb-doped ZnS informed by the understanding of how a NC forms, and exploring the variables that can be changed to alter the product of the synthesis. In order to fully understand and control doping, first the nucleation and growth of an NC must be understood. A literature review of this

topic is presented in Chapter 2. Hot injection and heat up synthesis methods will be employed to possibly synthesize doped NC. The results of these syntheses may be one or a combination of the following four products:

1) ZnS NCs only

2) Mixtures of ZnS NCs and PbS NCs

3) ZnS NCs with Pb atoms incorporated into the bulk of the NC and/or absorbed onto the surface of the NCs. The synthetic milieu may or may not also contain PbS NCs.

4) Core-shell structures. In core-shell structure, ZnS NC cores may be shelled with a mono- or multi-layer of PbS NC. This could also happen in reverse, where a PbS NC core is shelled by a mono- or multi-layer of ZnS NC.

Any one of these could be possible due to the differences in growth rates and stabilities of PbS and ZnS NCs. Any given doping trial may contain any one of these products. The syntheses described here are likely not proceeding under equilibrium conditions, so the products realized may not always be the most energetically stable products. Further discussion of possible products can be found in the following chapters.

Variables, such as temperature of Zn flask, temperature of Pb flask, and mole ratio between Pb and Zn, were altered in attempt to both achieve and control Pb doping. Products of doping were characterized using infrared (IR) spectroscopy, ultraviolet-visible (UV-Vis) spectroscopy, fluorescence spectroscopy, transmission electron microscopy (TEM), and energy dispersive x-ray spectroscopy (EDS). The

experiments described here are informed by preliminary work conducted by Dylan Perraut.[14] The key hypothesis of this thesis is that by controlling synthetic variables, successful doping can be achieved and controlled. This work is not an exhaustive body of all possible synthetic approaches but rather a broad exploration of key synthetic variables that will inform the work of further researchers.

CHAPTER 2

REVIEW OF THE SYNTHESIS AND GROWTH OF BINARY CHALCOGENIDE NANOCRYSTALS

2.1 General Overview of Nanocrystal Synthesis

The goal of this research is to synthesize colloidal zinc sulfide (ZnS) NCs substitutionally doped with Pb^{2+} ions. It is necessary to understand how the NCs are formed in order to manipulate the NCs' synthesis to include the desired dopant in the final product. Two of the control syntheses used in these experiments are those of lead sulfide (PbS) NCs and ZnS NCs. The PbS NC synthesis proceeds via hot injection synthesis, where the S precursor is injected into a hot solution of Pb precursor. The ZnS NC synthesis is a heat-up synthesis technique, which allows the S precursor and the Zn precursor to be in the same reaction vessel and heated slowly.[15] Understanding how NCs form at the atomic level, specifically PbS NCs and ZnS NCs, affords strategic methods for the addition of the dopant ions.

The atomic level formation processes for the NCs is thought to be very similar for both the hot injection method and the heat up method. **Figure 2.1** shows these steps for a heat-up synthesis. The general steps are 1) precursor formation, 2) monomer formation, 3) nucleation, and 4) growth processes that yield NCs. Any differences between the two methods will be pointed out in the following section. If no mention is

made of differences then it can be assumed that the two methods follow the same processes.
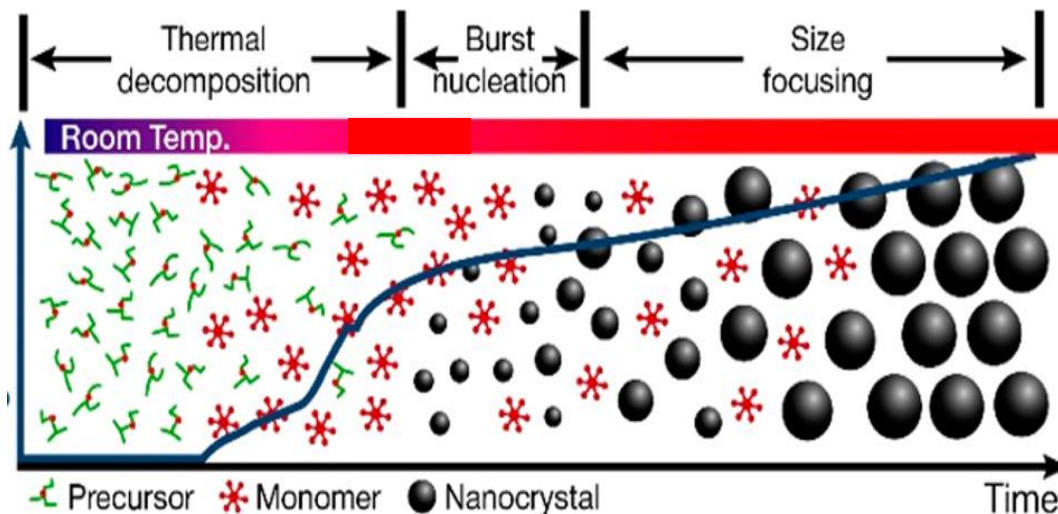
Figure 2.1: Monomer formation in a heat up synthesis occurs as temperature increases. In a hot injection synthesis, the metal and sulfide monomers would form in separate vessels. Source: Carey, G.; Abdelhady, A.; Ning, Z.; Thon, S.; Bakr, O.; Sargent, E. *Chem. Rev.* **2015**, *115*, 12732–12763.

2.2 Precursor Formation

The hot injection synthesis of PbS was developed by Hines et. al.[16] A Lead – oleic acid complex known as lead oleate ($Pb(OA)_2$) was the metal precursor used in PbS synthesis. This precursor formed when lead oxide was heated under vacuum in the presence of excess oleic acid as shown in **Figure 2.2**. Since the reaction starts with a lead oxide reagent, the complexation with oleic acid is performed under vacuum to remove

the displaced oxygen from the reaction vessel. Many metal oxides are stable under the reaction conditions used here, so removal of the molecular oxygen is essential so that no side products are formed.

PbO + Oleic Acid $\xrightarrow{\triangle}$ Pb – Oleate Complex
(C$_{18}$H$_{34}$O$_2$) + O$_2$ (g)

Pb – Oleate Complex + [structure] $\xrightarrow{\triangle}$ PbS Nanocrystals
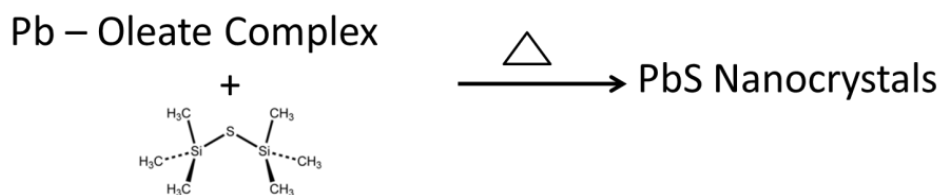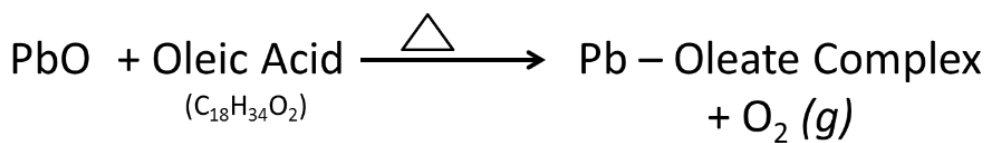
Figure 2.2: The reaction scheme for the hot injection synthesis of PbS NCs using the Hines et al. method.

Four binding modes for the lead oleate complex were discussed by Cass et al.[17] The binding modes are shown in **Figure 2.3**. IR analysis showed that chelating and bridging bidentate binding modes are the most common. In their work, the asymmetric O-C-O stretch for the bridging ligand appeared at 1535 cm^{-1}. The asymmetric O-C-O stretch for the chelating ligand appeared at 1525 cm^{-1}.

20

Figure 2.3: Binding modes of the Pb precursor. Source: Cass, L. C.; Malicki, M.; Weiss, E. a. *Anal. Chem.* **2013**, *85*, 6974–6979.

The heat up synthesis of ZnS was published by Zhang et al.[18] The reaction scheme for this synthesis is shown below in **Figure 2.4**. A zinc-oleylamine complex (Zn(OLA)$_2$) was the metal precursor used in the ZnS synthesis. This precursor formed when zinc stearate was heated under inert gas in the presence of oleylamine. IR spectra indicate that a zinc-oleylamine complex has formed. When a metal – nitrogen bond is formed the –NH$_2$ asymmetric stretching peak will shift from ~3389 cm^{-1} to a slightly lower frequency indicating that the nitrogen is bound.
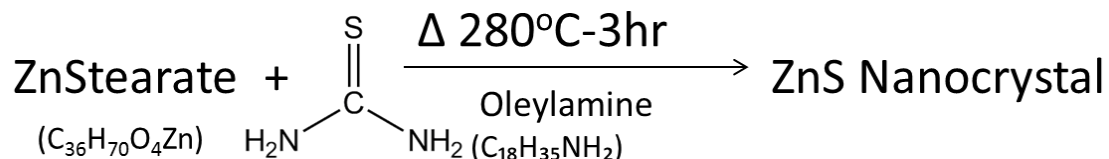
Figure 2.4: The reaction scheme for the heat up synthesis of ZnS NC using the Zhang et al. method

The sulfur precursor was bis(trimethylsilyl)sulfide in the PbS synthesis and thiourea in the ZnS synthesis. It is helpful to choose a very highly reactive sulfur reagent for the sulfur precursor so that this precursor can rapidly form monomers, which lead to small NC clusters.[19] The sulfur precursor that forms when sulfur is heated with alkylamines is discussed by Thomson et al.[20] In that work, nuclear magnetic resonance spectroscopy (NMR) was used to determine what sulfur compound(s) exist prior to NC nucleation and growth. They determined that the most prevalent sulfur – oleylamine precursor is an alkylammonium polysulfide. Then, with continual heating, the alkylammonium polysulfides will break apart again to form H_2S, which can then form monomers and react with metal monomers to form NC.[20] Thus, sulfur precursor formation is a multi-step process. We assume that H_2S precursors are also formed in the presence of oleic acid.[20]

Oleic acid and oleylamine serve as coordinating solvents in the PbS and ZnS synthesis respectively. Coordinating solvents are extremely useful for many reasons. First, coordinating solvents complex the metal ions to form the precursor. Throughout the nucleation and growth stages, the coordinating solvent serves as surface capping ligands on the NC surfaces to prevent the formation of bulk crystals and to afford solubility. Surface ligands can also be helpful in enhancing the photoluminescence yield and controlling the energy of the excited states in the NC.[19] IR spectroscopy from Cass et al. determined that there is a 1:1 ratio of chelating to bridging oleic acid ligands on the surface of a PbS NC.[17]

22

2.3 Monomer Formation, Nucleation, & Growth

Once the precursors form, energy supplied in the form of heat causes the precursors to break apart to form free ions (Zn^{2+}, Pb^{2+}, S^{2-}). Because NCs consist of repeating ions, these ions can be thought of as monomers in solution. Monomer creation is depicted in **Figure 2.1**. During a PbS hot injection synthesis, lead oleate is heated to yield the lead monomer before the injection. Sulfur monomers do not form until the sulfur mixture is injected into the lead solution. Once injection occurs, sulfur monomers form quickly due to the high energy from the heat. In a ZnS heat-up synthesis, the zinc and sulfur monomers both form in the solution as it gains energy with the addition of heat.

Once monomers of the metal and sulfur species coexist in the reaction mixture, NC nuclei form. These nuclei are small clusters of ions—formed when a few monomers come together and bond to each other. These are ionic bonds forming so the reaction is usually exothermic, but input of energy in the form of heat is necessary during nucleation and growth in order to maintain the monomeric forms of Pb, Zn, and S. Plus, excess energy allows the ions to find their lowest energy conformations, yielding highly crystalline NCs. The energy contained in the bonds between monomers is referred to as the lattice energy. The lattice energies for PbS in the rock salt crystal structure and ZnS in the wurtzite crystal structure are 2995 kJ/mol and 3308 kJ/mol respectively.[21,22] Lattice energies reflect the amount of energy released as bonds form.

When nuclei formation occurs the entropy of the solution decreases. When monomers exist they are dissolved in solution, but when nuclei form they become solids suspended in solution. Once a critical number of nuclei form, it is more thermodynamically favorable for monomer to add to existing NC nuclei rather than to keep forming new nuclei. This adding of monomers to existing nuclei is called NC growth. Growth is energetically favorable compared to nucleation because growth has a less negative impact on the mixture's entropy. Nuclei formation and growth of NC in the heat up method occurs slowly relative to hot injection. In the heat up synthesis, precursors, monomers, and nuclei may all co-exist. In hot injection, nucleation cannot occur until all monomers are present in one flask (after injection). Thus, the nucleation and growth in the hot injection synthesis occur very rapidly and almost simultaneously. A more detailed explanation of thermodynamic and kinetic factors affecting NC nucleation and growth can be found in later sections of this chapter.

NC growth is thought to occur via several mechanisms, but there are two key mechanisms on which the community agrees. The first prominent mechanism was suggested by LaMer.[23] The LaMer mechanism can be divided into three different stages. In the first stage there is a rapid increase in the monomer concentration in the solution. (This first stage is only relevant for the heat up method.) In stage two the monomers go through "burst" nucleation where the concentration of monomer is lowered significantly corresponding to the increase in the number of nuclei. For a brief moment there is a fast rate of growth for the nuclei to reduce the overall concentration of nuclei.

This means that for a brief period some nuclei dissolve to add to the other nuclei, in an Ostwald ripening process. The amount of time that constitutes a "brief period" will depend on several factors including the material system, temperature, solvent, concentration, and largely surface ligand.[24] Due to the large number of factors the amount of time will vary. Then in the last stage of the LaMer mechanism, the growth of the NC occurs at a slow rate.[25]

The second NC growth mechanism was developed by Finke-Watzky.[23] This mechanism is only a two stage event, where nucleation and growth occur simultaneously. The two stages consist of a slow, continuous nucleation and at the same time, an auto-catalytic surface growth. Ultimately, monomer come together to form nuclei and at the same time monomer is adding to these nuclei for the growth of NCs. This process has never been exclusively proven, but has informed the kinetic fittings for several metals including platinum, ruthenium, and iridium.[23]

Regardless of the nucleation and growth mechanisms, Ostwald ripening has been observed for colloidal NCs.[24] Ostwald ripening occurs after the NC nuclei reach a critical size. Critical size is determined by monomer solubility within the surfactant, the sorption rate constant for the particular NC, the molar volume of the NC, and the surface tension.[24] When critical size is reached, smaller NCs break apart to provide monomers that add to larger stable nuclei, forming larger NCs. Ostwald ripening occurs because the smaller NCs have higher surface energy than the nuclei of the critical size.[23] Additionally, Ostwald ripening is responsible for the relatively narrow size dispersion

observed in colloidal NCs. Digestive ripening is the opposite of Ostwald ripening. This is where larger NC break apart to help with the growth of smaller NC. This, however, is not the likely case for the PbS or ZnS NC because of the decrease in surface free energy provided by the coordinating solvent.[23]

Once growth has occurred, the resulting stable NCs have metal-rich surfaces.[17] With a metal rich NC, the coordinating solvent can bind to the surface of the NC. The ligand that attaches to the outside of the NC can have an effect on properties of the NC, such as absorption, photoluminescence (PL), and redox activity. For instance, amines are widely known to increase the fluorescence quantum yield of colloidal semiconducting NCs. The ligand symmetry and energy can affect the energy of the lowest excited state of the NC; when symmetry and energy of the ligands and the NC match well, the diameter of the NCs is effectively increased. When ligand energy match the highest occupied and lowest unoccupied molecular orbitals of the ligand are energetically near the nanocrystalline frontier orbital energies. Matching in symmetry means that the highest occupied and lowest unoccupied molecular orbitals of the ligand is shaped in such a way that the constructive overlap with the nanocrystalline frontier orbitals is possible.

When the ligand symmetry and/or energy do not match could mean that the ligand is very labile, which could decrease the stability of the NC. When this occurs it is possible for the ligand to introduce mid-bandgap states that can be thermodynamically accessible to excited electrons, however, this creates a trapped state whereby the

photoexcited electron is "trapped" by a mid-bandgap state. This trapping event is not permanent, but essentially intercepts the photogenerated electron before it can make its way to the hydrogen ions. These states are referred to generally as surface states. The ligand can affect the redox activity because a redox active molecule must be able to reach the NC through gaps in the ligand attached to the outside of the NC. The degree to which a NC's redox activity is affected by ligands is determined by the density of ligands and the ligand packing structure rather than ligand length or degree of conjugation.[19]

2.4 Nanocrystal Formation Thermodynamics and Kinetics

Now that the NC syntheses have been described generally, a more detailed examination of relevant kinetics and thermodynamics can occur. As a NC forms over time, there are differences in types and amounts of available reagents, in the rates of monomer formation, nucleation, and growth, and in the size of NC. **Figure 2.5** depicts NC formation and the concentrations of various species during the heat up method, clearly showing the relative rates at which these species appear and are consumed. This data is based off calculations and simulations to provide an overview of the key reaction parameters in a heat-up synthesis. The hot injection method is very similar—the key difference is the immediate introduction of monomers afforded by hot injection rather than the gradual increase in monomer concentration during the heat up synthesis.

27
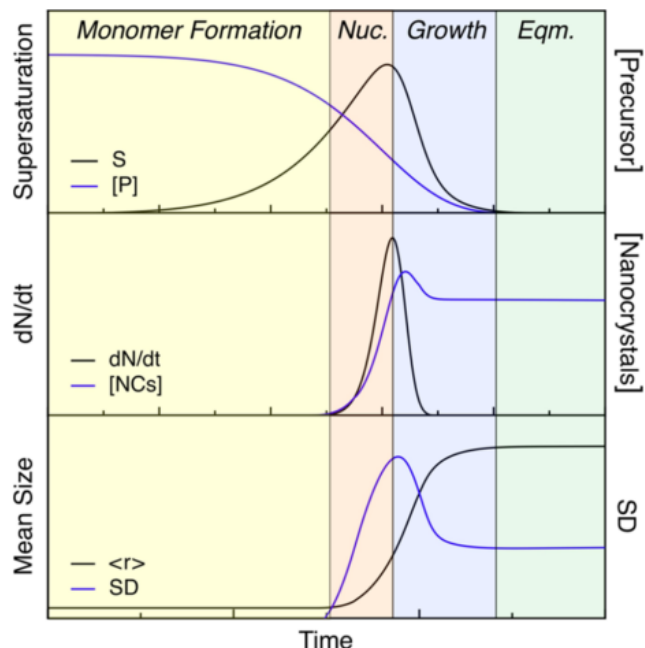
Figure 2.5: Graphical depiction of a wide variety of components during NC formation over time. S = supersaturation, [P] = precursor concentration, dN/dt = rate of nucleation, [NCs] = nanocrystals concentration, <r> = radius of NC, and SD = size distribution of NCs. Source: Van Embden, J.; Chesman, A. S. R.; Jasieniak, J. J. *Chem. Mater.* **2015**, *27*, 2246–2285

In **Figure 2.5**, the yellow section indicates the time period during which monomer formation occurs. The red section indicates nucleation is occurring, blue indicates growth, and green indicates that the solution has reached equilibrium. The lines depict an increase or decrease in concentration of a particular part of the NC formation process or a rate of occurrence of some factor.

As seen in the yellow top section of **Figure 2.5** the concentration of precursor (blue line) drops off at the end of monomer formation and continues to decrease

28

through nucleation and growth.[26] As the monomer concentration increases, the supersaturation of the solution (black line) with monomer increases. Once the solution is in equilibrium (between dissolving nuclei to afford monomers and growing nuclei), there is no more precursor present. The concentration of monomer increases with the input of heat and continues to increase through nucleation; these phases happen simultaneously as described by the Finke-Watzky mechanism. Monomer concentration drops off as growth begins because more monomers are being added to existing nuclei. Metal and sulfide monomers will return to the precursor form if the reaction is quenched by cooling before all the monomer is added to the NC.[26]

The rate of nucleation (dN/dt, middle panel of **Figure 2.5**) is important when discussing the kinetics of this reaction. The nucleation period is marked by a rapid increase in the number of nuclei (blue line) afforded by the high availability of monomer (represented by S, the degree of supersaturation). The rate of nucleation (black line) increases dramatically during the nucleation time period as several NCs nucleate. Once the reaction reaches the growth stage and it becomes more favorable for monomer to add to existing nuclei rather than to create new nuclei, the rate of nucleation drops off significantly. The largest effects on the rate of nucleation come from the concentration of monomer present in the solution and the surface free energy of the NCs, afforded by the size and the coordinating solvent.[23] The more monomer present the faster the rate of nucleation until a critical concentration of nuclei is reached. If less monomer is present the rate of nucleation will also be slower. The variation in surface free energy

29

comes from the coordinating solvent used and the size of the NCs.[23] When enough

nuclei reach the critical size, Ostwald ripening occurs and the smaller NC break apart,

thus decreasing the concentration of total NC.[26] The total concentration of NC drops off

a little in the growth stage, then levels out.

The bottom panel of **Figure 2.5** shows the radius of the NCs (black line) and the

size distribution (blue line) throughout the NC synthesis. Ostwald ripening is the reason

for the larger drop off in size distribution during the growth and equilibration phase.

There is a wide variety of size distributions until Ostwald ripening takes over and the size

distribution is decreased as more monomers are available to add to larger NC and the

concentration of NC diminishes.[26]

Another way to discuss the entire NC formation process is to talk about it both

kinetically and thermodynamically. As can be seen in **Figure 2.6**, precursor becomes

monomer with the addition of heat at some rate of formation (k_f). Monomers become

nuclei with the addition of heat at a different rate, the rate of nucleation (k_n).[26] The

process of monomers becoming nuclei is driven by the addition of heat in both synthesis

methods as well as the increase in monomer concentration in the heat up method. The

monomer concentration will, at some point, become so large that the reaction will

move forward into the nucleation phase. Then monomer will add to existing nuclei with

the addition of heat at still another rate. As a NC grows, monomer diffuses to the

particles-solution interface, which exists between the NC and the solution around it.

When the monomer reaches the particles-solution interface it may be met by its

counterpart--Pb^{2+} or Zn^{2+} meet S^{2-}, or S^{2-} meets Pb^{2+} or Zn^{2+}--or it may not. If the

monomer does meet its counterpart, then the NC will grow at a certain rate of growth

(k_g). If the monomer does not encounter its counterpart, then the monomer will diffuse

from the particle-solution interface at some other rate of diffusion (k_d).[26]

$$\text{Precursors} \xrightarrow[k_f]{\Delta} \text{Monomers} \xrightarrow[k_n]{\Delta} \text{Nuclei}$$
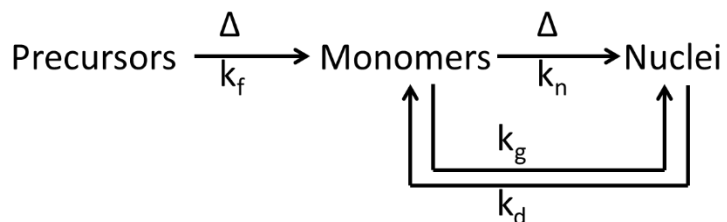
Figure 2.6: Rate constants for the nucleation and growth of NCs where Δ = heat, k_f = the

rate of formation, k_n = the rate of nucleation, k_g = the rate of growth, and k_d = the rate

of diffusion.

These last two rate constants shown in **Figure 2.6** are k_g and k_d, and these are

influenced by Ostwald ripening, which occurs because monomers can absorb to and

desorb from the NC surfaces. Adsorption of monomer to the NC is dependent on the

concentration of monomer in solution; however, desorption of monomers from the NC

depends on many more factors. Some of these factors include the radius of the NC, the

surface tension of the NC and the solubility of the NC, which is determined by the

coordinating solvent.[24]

This entire process can be explained thermodynamically as well. Two equations

can generally describe the thermodynamic considerations of NC formation. In Equation

(2), the species identified as products and reactants change depending on the particular part of NC formation being discussed. For instance, when discussing precursor breaking down to form monomer, the product would be monomer, and the reactants would be the precursor. However, if discussing the formation of small nuclei from monomers, the products would be the nuclei and the reactants would be the monomer.

$$\Delta G \; \alpha \; \ln \; [\text{products}]/[\text{reactants}] \qquad (2)$$

$$\Delta G \; \alpha \; \Delta H - T\Delta S \qquad\qquad (3)$$

In both equations, ΔG stands for Gibbs free energy, ΔH stands for enthalpy, and ΔS stands for entropy. ΔG is proportional, rather than equal, to the other factors in Equations (2) and (3) due to a wide variety of other considerations in the complicated reaction matrix including the surface free energy and lattice energy. If ΔG is positive, the reaction is nonspontaneous, and thus requires the addition of energy (usually in the form of heat) to further the reaction. If ΔG is negative the reaction is spontaneous, meaning that no energy input is required. For NC formation, the ΔG for the reaction is almost always positive; monomer formation is particularly energy intensive. As the amount of reactants (monomers) increase, the ΔG becomes smaller and the reaction will shift toward the products (nuclei), as seen in Equation (2).

In Equation (3), ΔH is the enthalpy of the reaction. This term has to do with the heat that is transferred to and from the NC during its formation, including the formation of precursor and monomer. An increase or decrease in ΔH will ultimately have an effect on the ΔG of the reaction. When ΔH is positive, the system absorbs heat and the

32

reaction is endothermic. When ΔH is negative the reaction will give off heat and the reaction will be exothermic. Most NC syntheses, including the formation of PbS and ZnS, are endothermic since there is an addition of heat to a reaction, specifically in the precursor transformation to monomer, as heat is required to break the bonds. Heat is released when bonds are formed—during the nucleation and growth stages. Again, this energy primarily affords the necessary monomers, though some of the energy also aids reorganization of ions in the crystals.

ΔS stands for the entropy of the reaction and is a measure of order vs. chaos. For instance, the molecules in a liquid are more chaotic than the molecules in a solid, which are held more rigidly. The universe tends to favor chaos, and ΔS is higher when the reaction matrix is more chaotic. Then, ΔS decreases when the reaction matrix is more ordered. The largest decrease in ΔS during NC synthesis occurs when monomers form nuclei. Monomers are dissolved ions in solution, so their chaos is fairly high. Whereas, nuclei are suspended solids in solution, so they are much more ordered. This shift from chaos to order, from high ΔS to low ΔS, is not favored. At this point ΔG increases which leads to a less favorable reaction. For this reason, in order for the NC synthesis to occur and for the monomers to come together to form nuclei, a large amount of heat must be added to the solution to overcome this low ΔS and high ΔG. The entropy is also important when keeping monomers as monomers, as ions are highly reactive species. Growth in NCs, as opposed to just nucleation, is favorable as reflected in the lattice

energy; a given NC nucleus will become more stable with the addition of more ions and more bonds to the NC.

Now cumulative impacts of the factors contributing to the difference between ΔH and ΔS will be considered. During monomer formation the ΔG increases until the activation energy is reached for the nuclei to form, which is also the highest ΔG reached in the NC synthesis, as shown in **Figure 2.7**. After nuclei formation occurs, the ΔG drops significantly due to the thermodynamic favorability of monomer addition and growth. The ΔG also decreases because of Ostwald ripening and the smaller, more thermodynamically not favorable, nuclei break apart to add to the larger, more thermodynamically favorable, NC. There is a critical free energy, seen in **Figure 2.7**, which is the highest amount of free energy required for stable nuclei to form.[23]
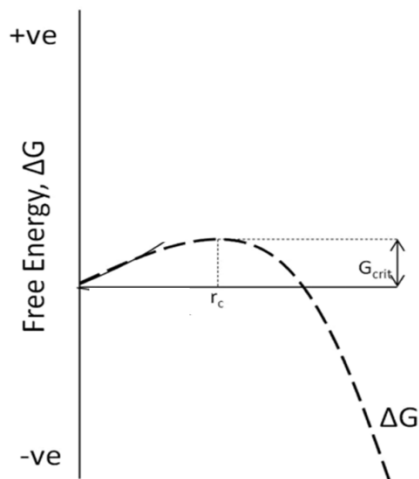
Figure 2.7: ΔG as the reaction progresses. G_{crit} = the most endothermic ΔG, r_c = the minimum size at which a nuclei can survive without being redissolved. Source: Thanh, N. T. K.; Maclean, N.; Mahiddine, S. *Chem. Rev.* **2014**, *114*, 7610–7630.

2.5 Conclusions

The heat up synthesis of ZnS and the hot injection synthesis of PbS are very similar in many ways. However, the difference between them can be simplified by saying that monomer accumulation alone cannot be a driving force for nucleation in the hot injection method, thus heat plays a more critical role in this method. Also, in the PbS hot injection synthesis, the nucleation and growth steps occur faster and simultaneously, relative to the same steps in the ZnS heat up synthesis. It is important to understand how NCs are made so that successful doping may be achieved. By understanding how a NC forms, the ideal time to insert the Pb^{2+} may be derived.

The work expressed here is a preliminary attempt at doping. It is important to attempt the simplest method that has a reasonable chance of doping success before crafting more complicated syntheses. As such, Pb^{2+} was introduced during the growth stage. The growth stage will continue until the temperature of the reaction decreases or until all reagents are consumed. While this may result in a mixture of ZnS and PbS NCs, doping may also occur. Even as NCs grow, there are atoms bonding to or dissociating from the NCs surface due to the ripening mechanisms discussed above. The NCs are growing quickly, so Pb^{2+} could interact with highly reactive surface sites on the ZnS NCs. If no further NC growth occurs after the Pb^{2+} absorbs to the ZnS surface, the resulting NC would be surface doped. Or, if the subsequent growth of the ZnS NC does occur after the Pb^{2+} absorbs to the ZnS surface, the Pb^{2+} may be trapped within the ZnS bulk. This work is designed to determine if the surface and/or bulk doping can be achieved by

injecting lead during the ZnS NC growth stage. Future students may examine other doping methods.

Based on the mechanisms and processes outlined here, we hypothesize that successful synthesis of Pb-doped ZnS NCs is probable when the Pb^{2+} monomer is injected into the ZnS solution during the NC growth stage (even if PbS NCs form simultaneously). This is because of the fact that NCs will continue to grow until the temperature is decreased or all reagents are consumed. The trials undertaken in this work are based on this hypothesis and while Pb incorporation was not measured directly, the fluorescence was measured and compared to that of controls.

CHAPTER 3

MATERIALS AND METHODS

3.1 Introduction

This chapter will discuss the synthesis methods of the NC controls as well as the doped trials, including variables altered in doping trials. Characterization techniques used to evaluate the efficacy of the synthetic attempts will also be discussed. Optical and electronic properties were examined with ultraviolet-visible (UV-Vis) and fluorescence spectroscopies, while structural properties were examined with infrared (IR) spectroscopy, transmission electron microscopy (TEM) and energy dispersive spectroscopy (EDS).

3.2 Schlenk Line

A Schlenk line is a special piece of glassware that allows an individual the ability to run a reaction under either an inert gas, such as N_2 *(g)* or Ar *(g),* or under vacuum, because any O_2 *(g)* present in the reaction vessel may react with the reagents used in the synthesis and force the formation of undesired products. The Schlenk line was set up in the lab as pictured below in **Figure 3.1**.

Figure 3.1: The Schlenk line set-up in the experimentation hood. In Pb-doped ZnS NCs synthesis the flask on the left is the Zn reaction flask, on the right is the Pb precursor flask. The Pb precursor flask is injected into the Zn reaction flask.

3.3 Synthesis of PbS NCs via Hot Injection

Lead sulfide nanocrystals, PbS NCs, were synthesized for use as controls using a method published by Hines et al.[16] In this synthesis, one 100 mL Chemglass three neck round bottom flask is filled 0.18 g (8.1×10^{-4} mol) of PbO (Sigma Aldrich, 99.9%), 0.25 mL (7.9×10^{-4} mol) oleic acid (OA, Matheson, Coleman, and Bell, ACS Grade) and 7.5 mL (0.023 mol) octadecene (Sigma Aldrich, 95%). The flask containing these compounds will be referred to as the "Pb reaction flask." Here, it is important to note that Pb is very toxic and extreme caution is required when dealing with the element. Careful cleaning

of all surfaces with chloroform (ACS grade) and other solvents are required for any surface that Pb touches.

The Pb reaction flask was attached to a condenser on the Schlenk line and was allowed to stir under vacuum while being heated to 150 °C using a sand bath over the course of one hour. The other two necks of the three neck flask were fitted with septa. When the compounds dissolved the mixture appeared a clear golden yellow, however, after continued heating the solution turned clear and colorless. With the addition of heat the PbO and oleic acid form a lead oleate complex, also known as the Pb precursor. The Pb to oleic acid ratio was higher than 1:2 to allow for excess OA, due to the formation of the precursor, $(Pb(OA)_2)$. With the addition of even more heat the precursor will break apart to form single Pb^{2+} ions, known as monomer. This happens via the reaction pathway depicted in **Figure 2.2**.

Another 50 mL Chemglass three neck round bottom flask, referred to as the "injection flask," was prepared containing the sulfur reagents 25 minutes prior to the completion of the reaction flask's heating. The injection flask contained 84 μL (4.0×10^{-4} mol) of bis(trimethylsilyl)sulfide (TMS, Acros Organics, 95%) and 4 mL (0.012 mol) of octadecene. TMS is extremely odorous and must be handled with care, *always* in the vacuum hood to ensure the smell cannot travel far. The injection flask was attached to another condenser on the Schlenk line and was allowed to stir under nitrogen gas flow at room temperature until the end of the one hour for the reaction flask.

Once the one hour of heating was complete the reaction flask was refilled with nitrogen gas to ensure positive pressure. A 30 mL capacity, needle-lock Luer Perfektum hypodermic syringe equipped with a 12 gauge, non-coring 6 inch stainless steel needle, acquired from Sigma-Aldrich, was used to pierce one of the septum of the injection flask. The needle is extremely sharp and must be handled with care. The syringe was purged with N_2 *(g)* by inserting the needle into the flask but not under the solution and drawing up the N_2 *(g)* then pulling the needle out and expelling the contents into the hood. This process was repeated three times to ensure the needle was rid of any oxygen. Then the needle was used to draw up all of the contents of the injection flask. The contents of the injection flask were then injected into the reaction flask by placing the needle through the septum and under the liquid line before releasing the contents of the injection flask into the Pb precursor/monomer solution. The release of the contents of the syringe must happen very quickly so that the nucleation start time is consistent for all NC. A few seconds after injection, the mixture turned black as PbS NCs quickly nucleated and grew. The mixture reacted for 3-5 minutes at 150 ˚C. To stop the NC growth, the reaction flask was then cooled in an ice bath.

After the reaction flask reached room temperature, the purification process began. The contents of the reaction flask were transferred to 50 mL polypropylene disposable conical centrifuge tube using minimal hexanes (ACS Grade) to wash the sides of the reaction flask. The centrifuge tube is shown in **Figure 3.2a**. The NCs are soluble in hexanes because their surfaces are coated with oleic acid. The tube was capped loosely

and sonicated briefly using a 1.9 L Fisher Scientific ultrasonic bath to disperse the NCs uniformly in hexanes. Excess acetone (ACS Grade) was added to the tube and the tube was centrifuged, on a Thermo Scientific Heraeus Multifuge X1 centrifuge, with a counter weight for 5 minutes at 5000 rpm. The centrifuge and counter weight are shown in **Figure 3.2b**. When the sample leaves the centrifuge it should look much like **Figure 3.2c**, with the NC deposited on the side of the centrifuge tube. The supernatant containing excess precursors and solvent was discarded, and the NCs were washed off of the sides of the tube with minimal amounts of hexanes. Again the tube was sonicated to ensure the NCs were dispersed and the process was repeated two more times with methanol (ACS Grade) instead of acetone. After the additional washes, the purified PbS NCs were stored in capped glass vials with minimal hexanes. The washes are intended to remove any metal or sulfur that has returned to the precursor form, as well as any excess coordinating solvent. The vial lids were wrapped with Parafilm to prevent evaporation of the hexanes. All glassware is thoroughly washed with many solvents including hexanes and chloroform, then placed in a base bath for further cleaning. The PbS NCs were characterized using UV-vis spectroscopy, fluorescence spectroscopy, TEM, and EDS.
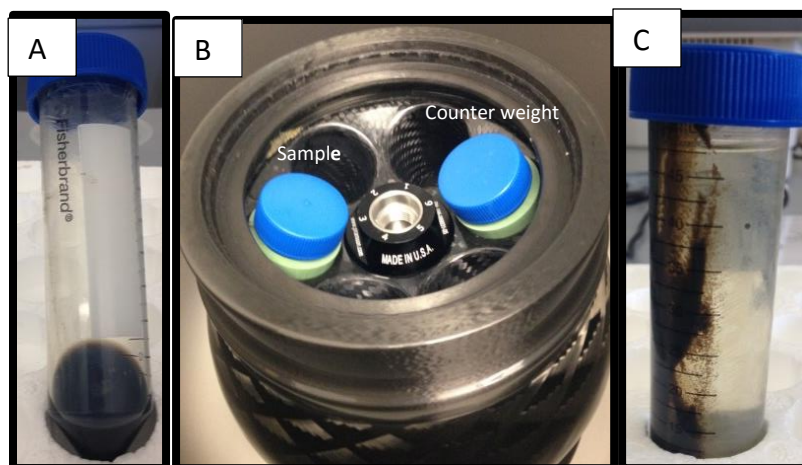
Figure 3.2: (a) A centrifuge tube containing NCs dissolved in minimal hexanes. (b) The centrifuge used in experiments with a sample and counter weight placed inside. (c) A centrifuge tube after centrifuging filled with acetone with NCs deposited to the side of the tube.

3.4 Synthesis of ZnS NCs via the Heat Up Method

ZnS NCs were synthesized for use as controls using a method published by Zhai et al.[18] The key difference between the PbS NC synthesis and the ZnS synthesis is that the ZnS NC synthesis is a one-pot synthesis. This means there was no injection and the entire reaction took place in one flask. The 100 mL Chemglass three neck round bottom flask contained 0.19 g (3.0×10^{-4} mol) zinc stearate (Alfa Aesar, 87.5%), 0.11 g (0.0014 mol) thiourea (ACS Grade), and 12 mL (0.0365 mol) oleylamine (OLA, Sigma-Aldrich, 98%). The reaction scheme is shown in **Figure 2.4**. The flask was attached to a condenser on the Schlenk line and placed in a heating mantle which allowed the

temperature to be adjusted through a Variac control system. The other two necks of the three neck flask were capped with septa. A thermometer was placed through one of the septa to monitor the temperature of the reaction mixture. The flask was allowed to stir under N_2 *(g)* flow, and heated for three hours to 280 °C at approximately 4.6 °C per minute—generally the reaction matrix reached 280 °C degrees at the end of the first hour. During the heating process, the reaction mixture turned a slight translucent yellow in color. After the three hours, the flask was removed from the heat to stop NC growth. The flask was allowed to cool to room temperature *without* the use of an ice bath. Since ZnS NCs are small, they don't absorb in the visible range. Because of this it is expected that the appearance of the reagents and the solvent will dominate, hence the yellow color which results from the unreacted sulfur and coordinating solvent. ZnS NCs cannot be observed until the reaction is cooled to room temperature.

Once the reaction mixture cooled, purification began. The purification of ZnS NCs is identical to that of PbS NCs, with one notable exception. Instead of the NCs being washed once with acetone and twice with methanol, for ZnS NC all three washes are with methanol. OA is more soluble in acetone but OLA is plenty soluble in methanol and does not need the extra solubility in acetone. This ensures that the final product is rid excess precursors and solvent. The ZnS NCs are stored the same as the PbS NCs are stored. After the purification process, the ZnS NCs were characterized using UV-vis spectroscopy, fluorescence spectroscopy, TEM, and EDS.

3.5 Synthetic Protocol for Lead Doping Attempts

The controlled synthesis of Pb-doped ZnS NCs has not yet been demonstrated, but the proposed optical and electronic properties of such NCs merit synthetic development. The following section describes attempts to synthesize Pb-doped ZnS NCs. Generally, ZnS NCs were synthesized as described above. Then, with 5 minutes remaining in the ZnS synthesis, lead reagent was injected into the reaction flask.[14] This was determined to be the best time for injection based upon trials run previously, where the Pb atoms were injected at several different times/temperatures.[14] In previous work, completed prior to the beginning of this project and conducted by Dylan Perraut, the lead reagent was injected at several different times and temperatures (from 20°C to 280°C). This was used to find an injection time based off of the UV-vis spectra produced, assuming that a spectrum that differed from a physical mixture of ZnS NCs and PbS NCs may indicate doping success. The UV-vis spectra of the injection at 280°C (5 min before end) showed a slight feature at about 540 nm that was different than all other times of injection. This work by Dylan Perraut provides the necessary justification for the injection time/temperature used.

The 5 min mark was experimentally determined to be within the growth stage for the following reasons: (1) the size dispersion of the NCs is consistent with that observed for NCs that have been through a growth stages and (2) the differences in variables affected the size but not the size dispersion. While the time at which growth begins was not explicitly measured, it was experimentally shown that the growth stage

had begun by examining the size and size dispersion of ZnS as a function of time and temperature.

The three synthetic variables tested in the doping attempts were the temperature of the ZnS reaction flask, the temperature of the injected lead reagent, and the lead to zinc mole ratio. **Table 3.1** summarizes all trials completed, and descriptions of these variations are given below.

Table 3.1: Doping Trial Attempts for Pb-doped ZnS

Trial	Date	Temp of Zn Flask (°C)	Mole Ratio (mol Pb:mol Zn)	Mole Ratio (mol Pb:mol S)*	Temp of Pb Flask (°C)
A	12/8/2015	280	0.3:1	1:15.6	20
B	12/9/2015	280	0.3:1	1:15.6	20
C	12/10/2015	230	0.3:1	1:15.6	20
D	12/16/2015	230	0.3:1	1:15.6	20
1	1/4/2016	200	0.3:1	1:15.6	150
1a	1/5/2016	200	0.3:1	1:15.6	150
2	1/7/2016	215	0.3:1	1:15.6	150
2a	1/13/2016	215	0.3:1	1:15.6	150
3	1/14/2016	230	0.3:1	1:15.6	150
4	1/19/2016	230	0.3:1	1:15.6	150
5	1/19/2016	200	0.5:1	1:7.82	150
6	1/21/2016	215	0.5:1	1:7.82	150
7	1/26/2016	230	0.5:1	1:7.82	150
8	1/26/2016	200	0.6:1	1:6.25	150
9	1/27/2016	215	0.6:1	1:6.25	150
10	1/27/2016	230	0.6:1	1:6.25	150
11	2/2/2016	230	1:1	1:4.45	150
12	2/2/2016	230	0.1:1	1:44.5	150
12a	2/5/2016	230	0.1:1	1:44.5	150
13	2/23/2016	280	0.3:1	1:15.6	150
14	2/23/2016	280	0.3:1	1:15.6	150

* Mole Zn : Mole S was 1.4 : 7 in all trials

These syntheses began like the synthesis of ZnS NCs described above. First, 0.19 g (3.0×10^{-4} mol) zinc stearate (Alfa Aesar, 87.5%), 0.11 g (0.0014 mol) thiourea (ACS Grade), and 12 mL (0.0365 mol) OLA (Sigma-Aldrich, 98%) were placed into a 100 mL Chemglass three neck round bottom flask. The Zn:S mole ratio was 1:4.7. This will be termed the Zn reaction flask. The Zn reaction flask was attached to a condenser on the Schlenk line and was heated to 200, 215, 230 or 280 °C for three hours under an inert gas (Ar *(g)* or N_2 *(g)*). The reaction mixture turned a clear yellow color upon continuous heating. This yellow color may result from unreacted sulfur and the coordinating solvent.

With one hour remaining in the Zn reaction flask heating time, the Pb precursor flask was prepared. The 50 mL Chemglass three neck Pb precursor flask contained 0.007 g, 0.02 g, 0.04 g, 0.05 g, or 0.07 g (3.14×10^{-5} mol, 8.96×10^{-5} mol, 1.79×10^{-4} mol, 2.24×10^{-4} mol, or 3.14×10^{-4} mol) of PbO and 12 mL OLA. The resulting Pb to Zn mole ratios were 0.1:1, 0.3:1, 0.5:1, 0.6:1, or 1:1 respectively. The Pb to S ratio is 1:44.5, 1:15.6, 1:7.82, 1:6.25, and 1:4.45 respectively. The Pb flask was attached to another condenser on the Schlenk line and was allowed to stir under vacuum for one hour at either room temperature or to 150 °C. The Pb flask appeared an opaque pale yellow in color.

With 5 minutes remaining in the Zn reaction flask heating time (2hr 55min elapsed), the Pb precursor flask was refilled with inert gas and the 30 mL syringe was purged with inert gas as described above. Using this needle and syringe, the contents of

the Pb flask were injected into the Zn reaction flask by drawing up the Pb precursor flask solution. The needle was quickly inserted into the Zn reaction flask and the tip of the needle was placed below the Zn solution before the Pb solution was rapidly released into the Zn reaction flask. A few seconds after injection, the solution turned a black or very dark brown. The reaction proceeded for 5 minutes, at which time the flask was removed from the heat and allowed to cool to room temperature. In some cases, the mixture turned a cloudy grey upon cooling. This seemed to happen when the Pb precursor flask was not heated before injection. In other cases, the solution remained its dark brown/black color. Note that in all trials, the total volume in the zinc reaction flask after injection of the lead reagent was 24 mL. It is unknown how much precursor remains unreacted after the 3 hours. Other students developed atomic absorption methods to determine this but these were not optimized by the completion of this project.

After the Zn flask reached room temperature, the purification process began. The contents of the Zn flask were transferred to 50 mL polypropylene disposable conical centrifuge tube using minimal hexanes (ACS Grade) to wash the sides of the reaction flask. The centrifuge tube is shown in **Figure 3.2a**. The NCs are soluble in hexanes because their surfaces are coated with oleic acid. The tube was capped loosely and sonicated briefly using a 1.9 L Fisher Scientific ultrasonic bath to disperse the NCs uniformly in hexanes. Excess acetone (ACS Grade) was added to the tube and the tube was centrifuged, on a Thermo Scientific Heraeus Multifuge X1 centrifuge, with a counter

weight for 5 minutes at 5000 rpm. The centrifuge and counter weight are shown in

Figure 3.2b. When the sample leaves the centrifuge it looked much like **Figure 3.2c**, with

the NC attached to the side of the centrifuge tube. The supernatant containing excess

precursors and solvent was discarded, and the NCs were washed off of the sides of the

tube with minimal amounts of hexanes. Again, the tube was sonicated to ensure the

NCs were dispersed and the process was repeated two more times with methanol (ACS

Grade) instead of acetone. After the additional washes, the purified Pb-doped ZnS NCs

were stored in capped glass vials with minimal hexanes. All glassware was thoroughly

washed with many solvents including hexanes and chloroform, then placed in a base

bath for further cleaning. The vial lids were wrapped with Parafilm to prevent

evaporation of the hexanes. Characterization included UV-vis spectroscopy,

fluorescence spectroscopy, TEM, and EDS.

Variation of the Zn flask temperature affected the amount of energy supplied

to the NCs during growth. Increased energy (heat) is known to correspond to increased

growth rates.[26] Differences in growth rates affect the size of the resulting NCs as well as

the extent of crystallinity in those NCs—both of which could afford (or prevent) doping.

Changing the mole ratio, specifically increasing the Pb concentration, increased

the probability of a Pb^{2+} ion colliding with a growing ZnS NC so as to facilitate doping.

Additionally, changes in the relative concentrations could affect the extent of doping—

the number of Pb^{2+} ions incorporated into a single ZnS NC. Finally, the relative Pb^{2+}

concentration in the reaction mixture may affect the formation of side products (PbS NCs, undoped ZnS NCs, etc.).

The temperature of the lead flask determined the chemical form of the lead at injection. When the lead flask was a room temperature, the flask contained PbO suspended in OLA. Upon heating, lead-OLA complexes formed. The Pb^{2+} ions possibly incorporated into the growing NCs come from the dissociated lead-OLA complexes. Thus, when the lead flask was kept at room temperature, lead-OLA and then Pb^{2+} ions form *after* injection into the Zn reaction flask. When the lead flask was heated prior to injection, lead-OLA complexes form *before* the Pb precursor was injected into the Zn flask.   Additionally, forming lead-OLA prior to injection allowed the removal of molecular oxygen. After the reactions have been run and the products have been purified, the characterization of the NC was performed. By using light from the UV-Vis portion of the electromagnetic spectrum, the NCs were analyzed for to assess optical and electronic properties relevant to photocatalytic H_2 (*g*) generation.

3.6 Characterization of NCs Using UV-Vis Absorbance Spectroscopy

An UV-Vis spectrophotometer uses light from a UV-vis light source, often tungsten and deuterium lamps. This light passes through an entrance slit, and then through a dispersion element which allows the light to be separated into its many wavelengths. The photons from the light pass through the exit slit to a quartz cuvette filled with the sample. Any light that is transmitted through the sample is collected by

the detector. An absorbance spectrum is displayed on the computer. A block diagram of

a UV-Vis spectrophotometer meter is shown in **Figure 3.3**.
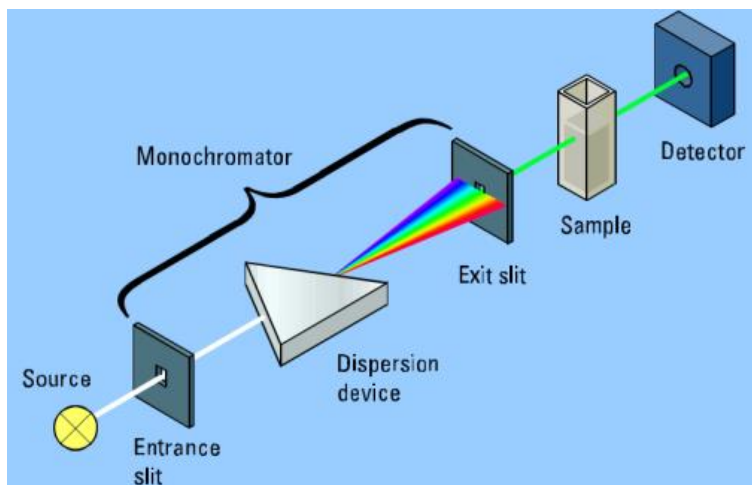
Figure 3.3: A diagram depiction of how an UV-Vis spectrometer works. Source: University, M. S. UV Visible Absorption Spectroscopy http://faculty.sdmiramar.edu /fgarces/LabMatters/Instruments/UV_Vis/Cary50.htm#Theory. (accessed Mar 1, 2016)

In this technique, 200 μL the NC samples were dispersed in chloroform (Pharmaco, 99.9%) was placed in a 1 cm^2 quartz cuvette. If the sample absorbs the light produced by the light source then very few, if any, photons will make it the detector and this will appear as an absorbance peak on the spectrum. If the sample does not absorb the wavelength of light then the detector will collect many photons of that wavelength and no peak will appear in this area on the spectrum.

If the NC sample absorbs the light, an electron will be excited from the VB to the CB. A NC will have a VB and CB that are separated by a band gap of a specific energy, which is determined by the chemical identity of the NC, the shape of the NC, the size of the NC, and the capping ligand. The light will give the electron energy, which will excite the electron from the VB and CB. This electronic transition is depicted in **Figure 3.4a**.
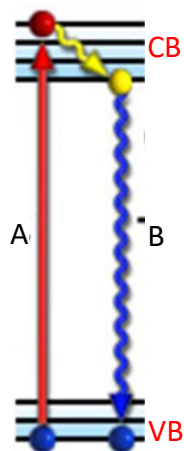
Figure 3.4: A Jablonski diagram depicting the VB and CB of a NC. (a) depicts the transition of an electron from the VB to the CB when a photon of appropriate energy is absorbed. (b) depicts the fluorescence of an electron from the CB to the VB. Source: Jablonski Energy Diagram, http://micro.magnet.fsu.edu/primer/java/jablonski /lightandcolor/ (accessed Feb. 15, 2016)

This excitation will occur at a certain range of wavelengths, and because the electron absorbed the light, little to none of the light will pass through the sample to the

detector. The UV-Vis absorbance for ZnS and PbS NC are well known, and shown in

Figure 3.5a-b. The absorbance of bulk Pb-doped ZnS NC has been measured as well. For

this reason, UV-Vis spectroscopy was helpful in characterizing the products of the

doping trials. The instrument used in all the characterization is a Cary 60 UV-Vis

spectrophotometer. The wavelength range was set to 200 – 1100 nm. The step size was

1 nm, the average time spent at a wavelength was 0.1 sec and the scan rate was 300

nm/min.
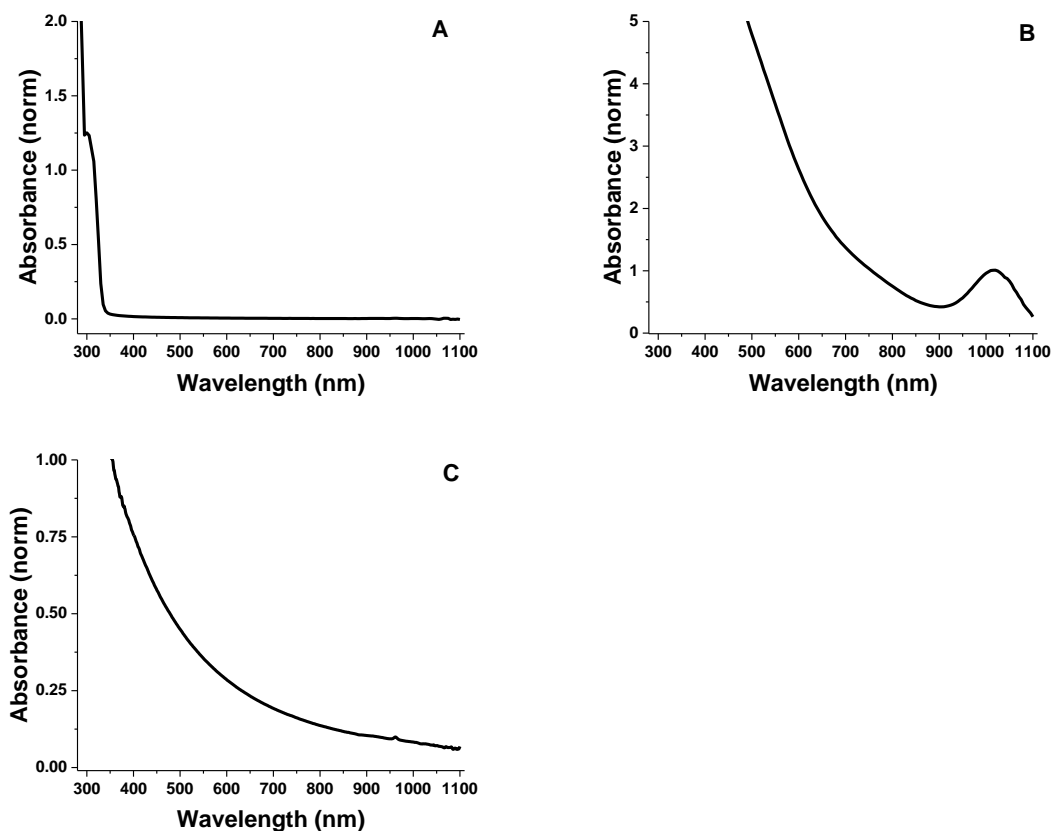
Figure 3.5: The UV-Vis spectrum of ZnS NC (a) shows an absorbance of ~315nm which is

consistent with literature. The UV-Vis spectrum of PbS NC (b) shows an absorbance of

the entire UV and Visible spectrum with a small hump at ~ 1024nm. (c) The UV-Vis spectrum of PbS and ZnS NC synthesized separately, then physically mixed together.

Figure 3.5a shows that ZnS NC do not absorb for most of the UV or visible spectrum. ZnS NC have an absorbance of ~315 nm, which is consistent with literature.[18] Figure 3.5b shows PbS NC with an absorbance ~1020 nm, which is also consistent with the literature.[16] The size of PbS NCs affect the placement of the ~1020 nm peak and it can shift from ~800 nm to ~1100 nm depending on the small or large size respectively. Figure 3.5c shows a physical mixture of PbS and ZnS NC. There are no identifiable peaks, but rather a gradual decrease in absorbance from 300-1100 nm.

3.7 Characterization of NCs Using Fluorescence Spectroscopy

Fluorescence spectroscopy is a complimentary characterization technique to UV-Vis spectroscopy. In this technique, the sample is also placed in a cuvette and placed in the instrument. A diagram of the fluorescence instrument is provided in Figure 3.6. The excitation light passes through the sample; here a range of 180 to about 800 nm was examined, though some instruments can go higher. If the excitation wavelength exceeds the bandgap energy, the sample will absorb some wavelengths of light just as in UV-vis spectroscopy. If a wavelength of light is absorbed, then an electron will be excited from the VB to the CB (Figure 3.4a). After a short time, the electron will relax back down to the VB (Figure 3.4b). As the electron falls, it releases energy in the form of light. This

emitted light is collected by the detector and a spectrum is produced. Fluorescence

spectroscopy detectors are oriented perpendicular to the excitation source and collect

the light emitted by the sample. UV-Vis absorbance detectors are oriented in line with

the light source and collect light transmitted through the sample. This is the key

difference between the two complimentary techniques.
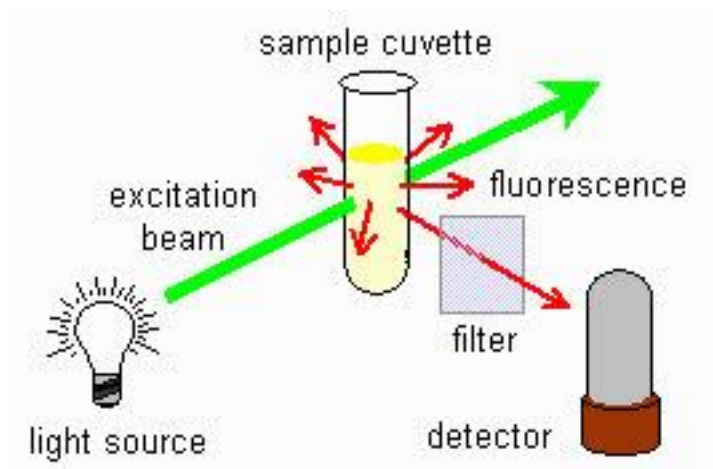
Figure 3.6: A diagram of how a fluorescence spectrophotometer works. Source:

Molecular Fluorescence Spectroscopy http://www.tissuegroup.chem.vt.edu/chem-

ed/spec/molec/mol-fluo.html (accessed Feb. 15, 2016)

If the spectra from a UV-Vis and fluorescence instrument were overlaid, the

fluorescence spectra would have a peak that is slightly red shifted, or higher in

wavelength, than its counterpart peak in the UV-Vis spectrum. This shift is called a

Stokes shift. A Stokes shift is the difference in nanometers between the absorbance

peak and the fluorescence peak wavelength. Stokes shift exists because the absorption and excitation of an electron happens extremely quickly (10^{-15} seconds). However, fluorescence takes quite a bit longer (10^{-9} seconds). Vibrational relaxation occurs such that the excited electron falls to the bottom of the conduction band before the excess energy is emitted.

The fluorescence spectrum of ZnS NC is known, and PbS NC does not fluoresce in the visible. The fluorescence emission spectrum of ZnS NCs are shown in **Figure 3.7a (black)**. A Stokes shift of about 46 nm between the absorbance and the emission spectra of the ZnS NCs is observed. The peak present at 355 nm is consistent with literature data and is representative of the main transition between the VB and CB of ZnS NC. This feature arises from the bulk ZnS, where each Zn and each S atom are fully coordinated. This allows the ZnS fluorescence to exhibit one narrow peak because the energies between these bulk atoms do not vary much. The peak present at 515 nm is indicative of a transition between surface state energy levels that exist on the surface of the ZnS NC. Zn and S atoms on the surface of the NC have different coordination than the bulk atoms. These surface atoms could have two uncoordinated bonds and two coordinated bonds, or any other arrangement. For instance, the Zn atoms on the surface may only be bound to three atoms instead of four if the purification process was too vigorous and capping ligands were inadvertently removed. For these reasons the peak at 515 nm is very broad—there are many different surface states that could exist over a wide range of energy levels.
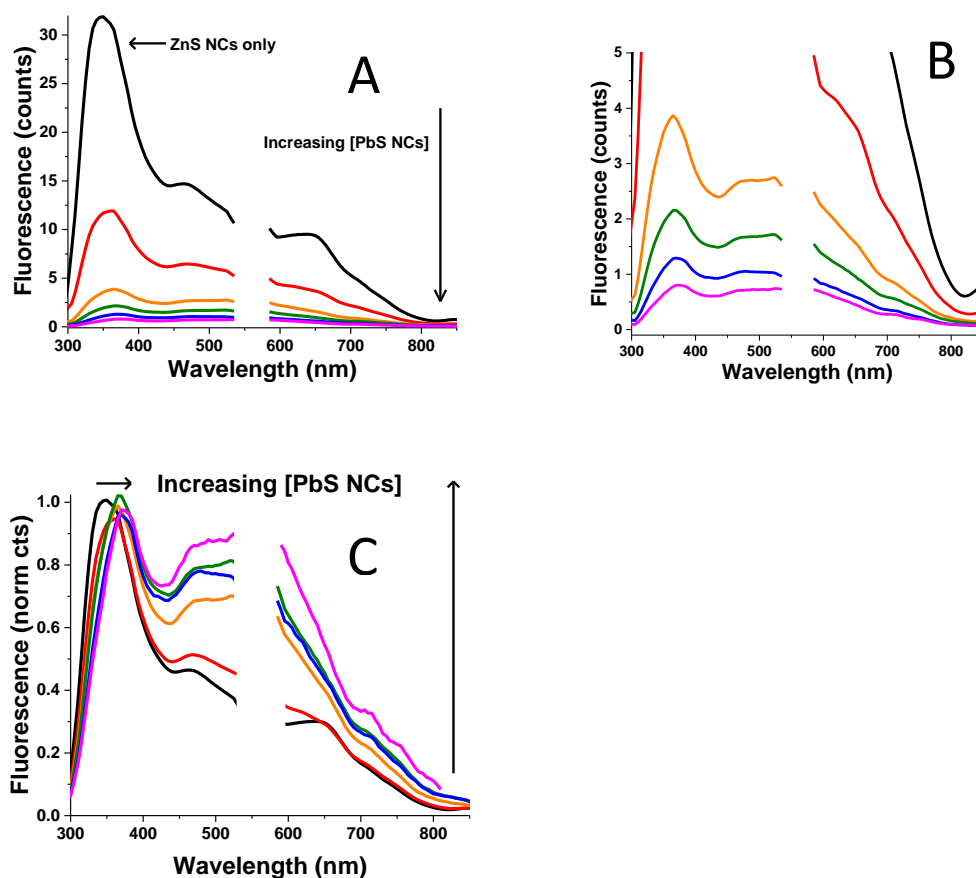
Figure 3.7: (a) Fluorescence spectra of ZnS NCs (black), ZnS NCs with 1 μL PbS NCs added (Red), ZnS NCs with 2 μL PbS NCs added (Orange), ZnS NCs with 3 μL PbS NCs added (Green), ZnS NCs with 4 μL PbS NCs added (Blue), and ZnS NCs with 5 μL PbS NCs added (Magenta). (b) Zoom in of Figure 3.7a. (c) Figure 3.7a normalized to the ~360 nm peak.

The fluorescence spectra depicted in **Figure 3.7** result from mixtures of separately synthesized PbS NCs and ZnS NCs. A fluorescence spectrum was first taken of ZnS NCs alone (**Figure 3.7** black). Subsequent spectra were collected as PbS NCs were

56

added. As more PbS NCs are introduced to the mixture, the overall emission of ZnS NCs at both ~360 nm and ~600 nm are decreased in intensity. Also note that the ZnS surface state emission is quenched more effectively than the bandgap emission with the addition of PbS NCs.

The fluorescence spectra of Pb-doped ZnS NCs is not known but is hypothesized to differ from that of a mixture of PbS NCs and ZnS NCs. For this reason, fluorescence spectroscopy will be helpful in the characterization of Pb-doped ZnS NC.

The fluorescence instrument used in all the characterization is Varian Cary Eclipse Fluorescence spectrophotometer. The wavelength range for the spectra displayed here were 290 – 1100 nm, with an excitation wavelength of 280 nm. This excitation wavelength was chosen from literature, also because it is always absorbed by the samples. The step size was 5nm, the integration time was 3 secs, and the scan rate was 100 nm/min. The excitation slit size was 10 nm, while the emission slit size was 5 nm. These slit sizes resulted in the best spectral quality while still maintaining a relatively small step size. Too large a slit size may lead to poor spectral quality because too much light is passed through the sample to the detector and separate peaks may begin to blend together. Too small a slit size will produce good spectral quality, but the acquisition time may become prohibitive (sometimes over an hour just for one excitation wavelength). It is important to note scattered light is also detected at the excitation wavelength and then at multiples of the excitation wavelength (i.e. excitation at 280nm, scattering peaks at 280 nm, 560 nm, and 840 nm). These peaks are not

related to the sample in particular and were removed from the spectra to allow for better interpretation.

3.8 Characterization of NCs Using IR Spectroscopy

Infrared (IR) spectroscopy was used to examine interactions between the coordinating solvent and the NC surfaces. IR spectroscopy involves IR light being passed through the sample, liquid or solid. As the NC absorbs that IR light, the bonds between the coordinating ligand and the metal begin to vibrate. Bonds have the ability to stretch and bend, both symmetrically and asymmetrically. The frequency at which these bonds vibrate is proportional to the energy required to vibrate that bond, and that energy is provided by IR light. The bond of interest when looking at the coordinating solvent is the metal – nitrogen, or metal – oxygen, bond for ZnS and PbS respectively. The mass of the metals should also be taken into consideration when trying to determine the frequency at which the metal and the coordinating solvent will vibrate. The frequency at which these bonds vibrate should change as function of being bound to a metal or not. Two IR spectra are shown in **Figure 3.8** depicting these metal – nitrogen (a) and metal – oxygen (b) bonds.
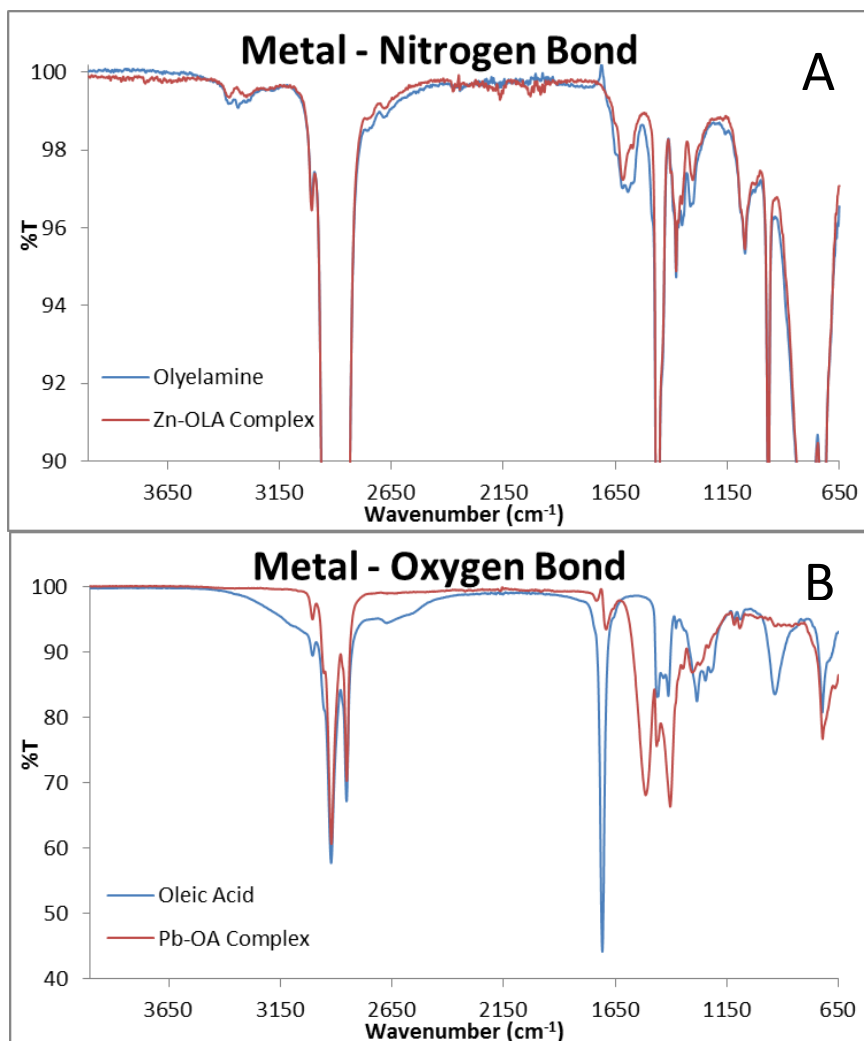
Figure 3.8: (a) IR spectra comparing free oleylamine (Blue) to a zinc bound oleylamine complex (Red). (b) IR spectra comparing free oleic acid (Blue) to a lead bound oleic acid complex (Red).

As seen in **Figure 3.8a,** the peak present in the oleylamine sample at ~3389 cm^{-1} is indicative of asymetretic stretching of the $-NH_2$. This peak is shifted in the zinc bound oleylamine complex.[18] This indicates that the Zn–OLA complex has formed by the zinc

metal attaching to two nitrogens on separate OLA structures. This data is consistent with the literature on Zn–OLA complex. Similarly, in **Figure 3.8b**, the appearance and strengthening of peaks at 1524 cm^{-1} and 1411 cm^{-1} in the bond Pb-OA complex are indiciative of the asymmetric and symmetric stretching of the O–C–O bond in the OA.[17] This indicates that the OA is bound to the metal and is consistent with literature data.

The asymmetric stretches of IR spectroscopy have been used in the past to determine the binding modes of the coordinating solvent to the NC. For this reason, IR spectroscopy will be used to show the binding modes that are present in the product as well as the identity of the precursor for Pb and Zn NC. The IR instrument used throughout the course of these experiments was a Perkin Elmer Spectrum 100 Fourier Transform with diamond attenuated total reflection (ATR).

3.9 Characterization of NCs Using Transmission Electron Microscopy

Transmission electron microscopy (TEM) allows the viewer to see images of stacks of atoms. This unique ability is afforded by the electrons smaller wavelength than that of visible light. A diagram of the inner workings of a TEM is provided in **Figure 3.9**.[28] TEM uses a beam of electrons generated from an electron gun, and this beam passes through a chamber held at ultrahigh vacuum conditions so that the electrons do not scatter off of any gaseous molecules. The electron beam then passes through a series of electromagnetic lenses that narrow the beam of electrons so that they can hit a small sample size. The beam of electrons must then pass through the sample. For this to occur

the sample must be extremely thin, less than 200 nm in thickness. After the electrons

pass through the sample, they will pass through another series of electromagnetic

lenses that will amplify the signal, and finally the electrons will hit a fluorescent plate.

This is needed because the human eye cannot see electrons and the fluorescent plate

fluoresces in the visible light spectrum where it can be seen by the human eye.
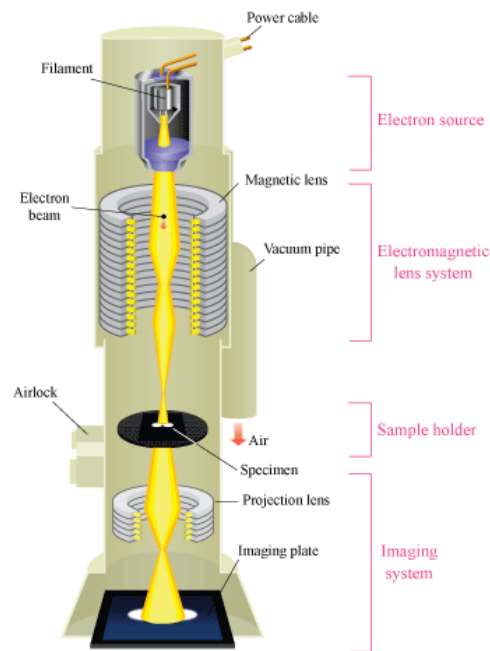
Figure 3.9: A diagram of a transmission electron microscope. Source: Basic Principles of

Transmission Electron Microscopy http://www.hk-phy.org/atomic_world/tem/

tem02_e.html (accessed Mar. 1, 2016).

The dark areas of the image are where the electrons did not make it to the fluorescent plate, which means they hit an atom and bounced in a different direction. The lighter portions of the image are where electrons made it through the sample without hitting anything and made it to the fluorescent plate. The larger the NC, containing more stacks of atoms, the better the image quality, because larger NC with more stacks of atoms affords more barriers for the electrons to hit and thus clearer images. These images were collected and compared for PbS NCs, ZnS NCs, and attempts to generate Pb-doped ZnS NCs to determine whether doping was achieved. The TEM images, taken by Dr. Dali Qian at the University of Kentucky Electron Microscopy Center, of PbS NCs and ZnS NCs are shown in **Figure 3.10**. The TEM used for these experiments was a Jeol 2010F with a 200 keV field emission gun. The TEM also has a Fischione high angle annular dark field detector (HAAFD) for Z-contrast STEM, which can give information about elemental composition and crystal structure at the atomic scale. Elements of higher atomic number appear darker due to the scattering of electrons on a HAAFD spectrum.
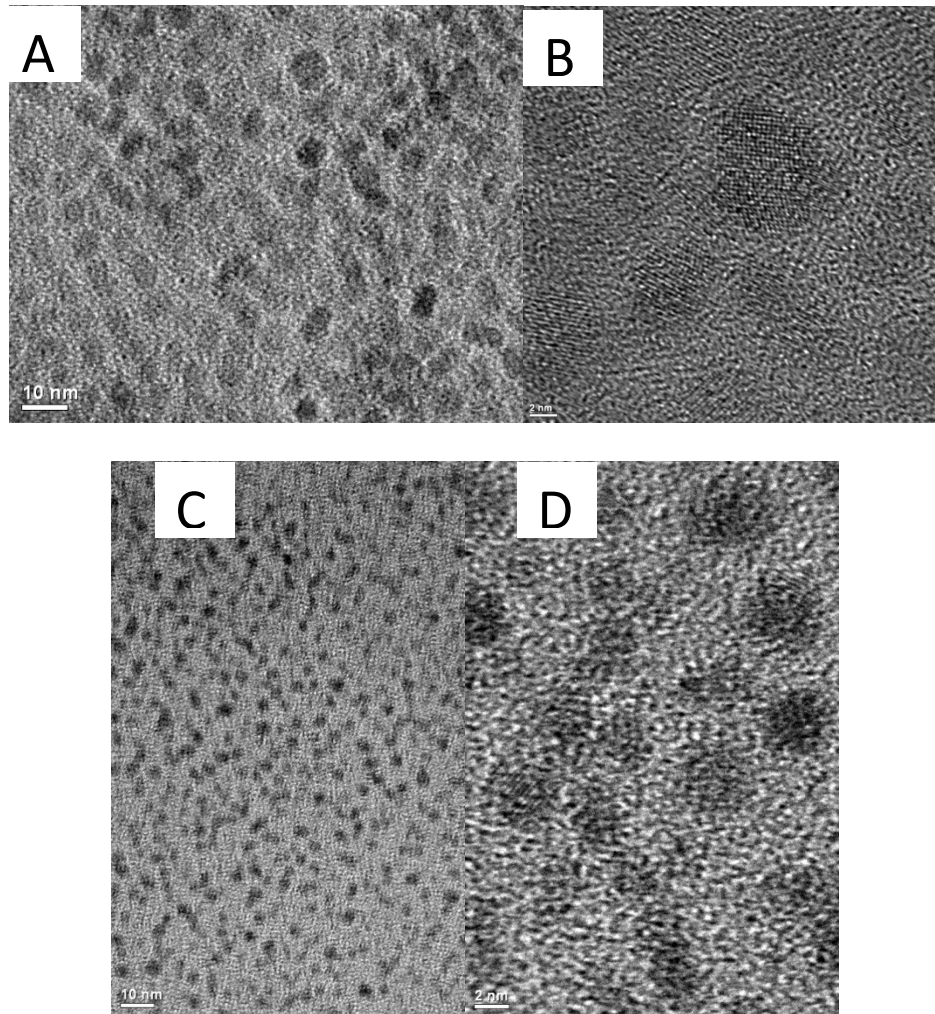
Figure 3.10: (a) TEM images of ZnS NCs and (b) a zoomed-in image of a few ZnS NCs. (c) TEM images of PbS NCs and (d) a zoomed-in image of a few PbS NCs.

As can be seen from the image in **Figure 3.10b**, the ZnS NCs are sufficiently large and a clear distinction can be made between rows and stacks of atoms. The PbS NCs displayed in **Figure 3.10d** look different from the ZnS NCs shown in **Figure 3.10b**.

Though the PbS NCs are not as large as the ZnS NCs, one can still see the distinct rows

and stacks of atoms that are in the NCs.

3.10 Characterization of NCs Using Energy Dispersive X-Ray Spectroscopy

Energy-dispersive x-ray spectroscopy (EDS) was used in tandem with the TEM.

EDS can be used to detect certain elements that exist in the NC. EDS uses the same

electron beam as the TEM. When the electrons pass through the sample they may hit an

atom. This collision causes the atom to eject one of its inner electrons. The atom then

replaces that inner electron with one from a higher energy level. As the new electron

falls in energy, it gives off its excess energy in the form of x-rays which are collected by

the EDS detector. Each x-ray is indicative of a certain element and even a certain shell

transition. The EDS used was an Oxford INCA EDX detector.

Relative concentrations of elements can be derived from the EDS spectrum. EDS

was run on PbS NCs, ZnS NCs, and trials for Pb-doped ZnS NCs. The EDS of PbS NC and

ZnS NC are displayed in **Figure 3.11**. The EDS that was used for the experiments was an

Oxford INCA EDX detector.
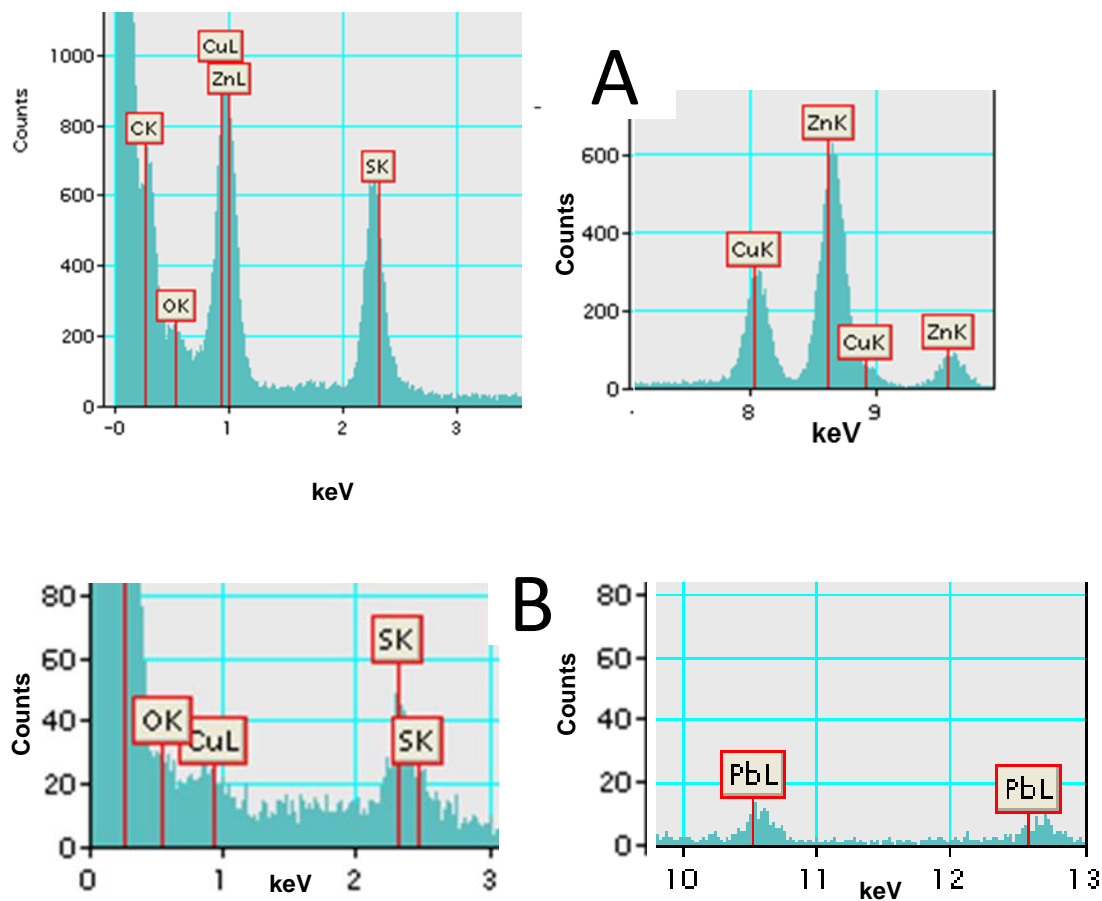
Figure 3.11: (a) The EDS data for ZnS NCs, where x-ray emission from Zn and S can be seen. (b) The EDS data for PbS NCs, where x-ray emission from Pb and S can be seen.

The EDS for ZnS NC show the presence of Zn and S in the sample. It also shows carbon, oxygen and copper. These are background elements that are present in every sample. The carbon also results from the long carbon chains acting as the coordinating solvent. The copper arises from the copper grid on which the samples are placed. The

oxygen could come from the metal oxidation, either the Zn, Pb, or Cu. The EDS shows

that the PbS NCs and ZnS NCs contain their expected elements appropriately.

CHAPTER 4

RESULTS AND DISCUSSION

4.1 Introduction

The purpose of this research was to synthesis and characterize Pb-doped ZnS NCs for use in H_2 *(g)* generation for solar energy applications. The synthesis of Pb-doped ZnS NCs was previously unreported, though literature suggests that bulk ZnS doped with Pb will have distinct optical properties measureable with absorbance spectroscopy and fluorescence spectroscopy. For instance, Tsuji et. al. doped Pb ions into bulk ZnS using successive ion layer adsorption techniques, and their spectra will be compared to those acquired in this work.[13] Doping trials were performed as described in Chapter 3, and the characterizations of the products are described and analyzed here. As with any novel synthesis there are a wide variety of undesired side products that may form in addition to, or instead of, the desired products (Pb-doped ZnS NCs). Possible undesired side products include, but are not limited to, mixtures of PbS NCs and ZnS NCs or a core-shell structures. In a core-shell structure, a small PbS NC may form, then ZnS NC form on the outside, encapsulating the PbS, or vice-versa with a ZnS core and a PbS shell. In order to qualitatively analyze synthetic products, spectra of the products obtained were compared to spectra of potential side products. If doping is accomplished, these spectra should show new features and they should look different from spectra of the undesired

products. More quantitative characterization was performed using electron microscopy

and energy-dispersive x-ray spectroscopy (EDS).

Generally, the doping trials involve 2 different flasks. The first is a Zn reaction

flask, containing the Zn and S precursors, is heated to afford NCs. The second flask

contains the Pb precursor; contents of this flask were injected into the Zn reaction flask

while the ZnS NCs were growing. These syntheses are described in detail in Chapter 3

and depicted generally in **Figure 4.1**.

Figure 4.1: The reaction scheme for the doping attempts conducted in this work. The Zn

reaction flask contained zinc stearate and thiourea in oleylamine; this flask was heated

to nucleate and grow ZnS NCs. The Pb precursor was prepared in a separate flask that

contained lead oxide in oleylamine. The contents of the Pb flask were added to the hot

Zn reaction flask to produce a mixture of PbS and ZnS NCs.

There were three variables altered in the experiments preformed as described in

Table 3.1. First, the Zn reaction flask temperature was varied from 200 ˚C to 280 °C; this

temperature controls the amount of energy available to the reagents during NC

nucleation and growth. The available energy effects the rates at which the NCs nucleate and grow; both of these processes are known to influence NC size, size dispersion, and crystallinity.[23,29] Additionally, the Zn reaction flask temperature may influence the degree to which the much larger Pb^{2+} ions are incorporated into the ZnS crystal lattice.

The second variable was the Pb precursor flask temperature, which was set to either room temperature (20 °C) or 150 °C before the precursor was injected into the Zn reaction flask. Varying the temperature of the Pb flask, which initially contains solid PbO and oleylamine, determines the composition of the Pb precursor injected. If the Pb flask contents are at room temperature when injected, the Pb precursor is likely a suspension of PbO in oleylamine. However, if the Pb flask is heated to 150 °C under vacuum before injection, the Pb exists primarily as lead oleate ($Pb(C_{18}H_{35}NH_2)_2$). Small amounts of Pb^{2+} monomer may also persist in this solution; any molecular oxygen generated during complexation is evacuated prior to injection. The oxygen may interfere with the other reagents, but the extent to which this does or does not occur is beyond the scope of this work.

The third variable examined was precursor ratios. The mole ratio of lead to zinc precursor (Pb:Zn) was systematically varied from 0.1:1 to 1:1. More Pb might lead to the formation of undesired products, such as distinct PbS NCs. However, less Pb also means the probability of doped product decreases, as the growing ZnS NCs may not come into contact with any lead.

69

The spectral data, electron micrographs, and energy dispersive spectra are presented below, organized by variable. Relevant control spectra are shown as needed. Summative analysis of all results follows the discussed data, and future directions for this work are discussed in Chapter 5.

4.2 Variable 1: the Zn Reaction Flask Temperature

The UV-Vis absorbance spectra as a function of the Zn reaction flask temperature are shown below. **Figures 4.2a-c** demonstrate the effects of Zn reaction flask temperature at mole ratios of 0.3:1, 0.5:1, and 0.6:1 Pb:Zn respectively. All of the purified NCs from these trials appeared a dark brown/black color. All of these spectra contain a peak near 360 nm, indicative of ZnS NCs. This feature reflects an electronic transition in ZnS NCs. Specifically, an electron in the ZnS NC valence band (VB) is photoexcited to the conduction band (CB) of ZnS NC. There is another feature present in these spectra that is not present in the controls—an inflection point near 610 nm, circled in **Figure 4.2a** for clarity. This feature is not an entirely new peak, but it is different from what was observed in the spectra for PbS NCs (**Figure 3.5b**), for ZnS NCs (**Figure 3.5a**), and for the physical mixture of PbS NCs and ZnS NCs (**Figure 3.5c**). A feature here is interesting (instead of a true peak) and hypothesized to correspond to doping because the dominate transitions occurring are still that of ZnS VB to CB and PbS VB to CB. Also, it is highly unlikely for all NCs to be doped, so any feature associated with doping is expected to be relatively weak in intensities. Tsuji et al. observed absorbance

features near 540 nm for bulk Pb-doped ZnS, similar to the absorbance feature observed near 610 nm in this work.[13] The feature at 540 nm was attributed to an electronic transition from filled Pb 6s states, which are introduced upon successful doping. While the feature observed in our work does differ from that observed by Tsuji et al, we do expect the absorbance of NCs to differ from that of bulk materials. This feature is suggestive of Pb doping, but it is not conclusive. Still, the absorbance spectra of these NCs do differ from those of ZnS NCs, suggesting that the NCs synthesized in these trials do differ from isolated ZnS NCs and isolated PbS NCs. In addition, this feature is well in the region of visible light, which means this photocatalyst will be able to absorb a large amount of sunlight to convert to H_2 *(g).*
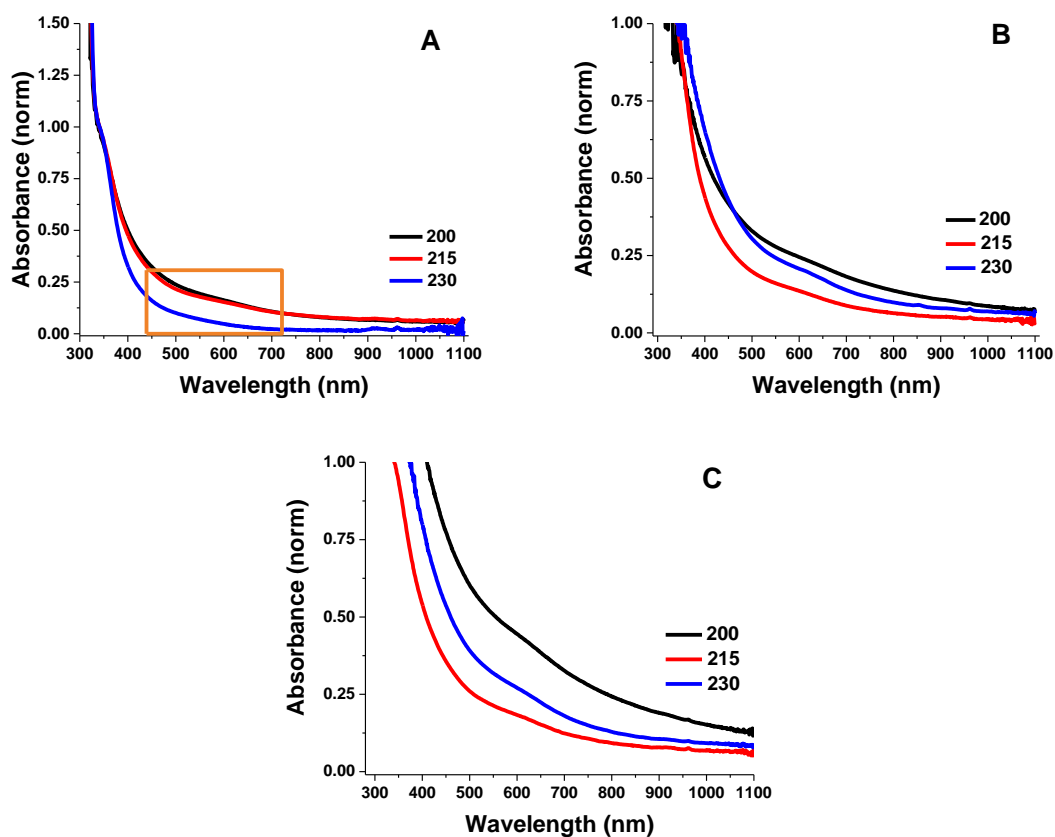
Figure 4.2: UV-Vis spectra of attempts at Pb-doped ZnS NCs with Zn flask temperature of 200 ˚C (black), 215 ˚C (red) and 230 ˚C (blue). Spectra (a) correspond to trials using a 0.3:1 Pb:Zn ratio, spectra (b) correspond to trials using a 0.5:1 Pb:Zn ratio, and spectra (c) correspond to trials using a 0.6:1 Pb:Zn ratio. The Pb flask temperature prior to injection was 150 °C in all trials.

The fluorescence spectra in **Figures 4.3** demonstrate the effects of Zn reaction flask temperature at mole ratio of 0.3:1. Overall, the intensity of these spectra is lower than that of isolated ZnS NCs, as Pb is known to quench ZnS fluorescence.[30] Still, the

fluorescence spectra from the doping trials do show similarities to that of the ZnS NCs spectra shown in **Figure 3.7a**. All spectra from doped trials show a peak at ~360 nm. This peak corresponds to the light emitted by an electron relaxing from the bottom of the ZnS NC CB to the VB, also referred to as bandgap emission. Also, all doped spectra show a broad peak centered near 600 nm. In ZnS NCs, this peak is indicative of NC surface states. These states arise from undercoordinated surface atoms and nonhomogeneous ligand passivation, which in turn create many electronic states in between the NC CB and VB. The peak is very broad because there are many possible surface states that differ in energy. The fluorescence spectra of ZnS show surface state emission centered near 515 nm, and the doping attempts show that peak red shifted about 85 nm to 610 nm.
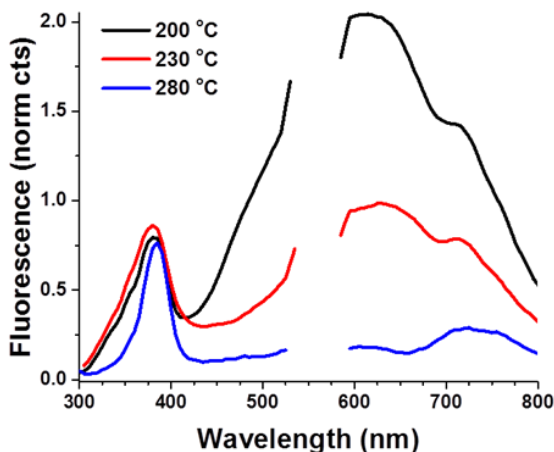
Figure 4.3: Fluorescence spectra, with excitation at 280 nm, of attempts at Pb-doped ZnS NCs with Zn reaction flask temperatures of 200 ˚C (black), 230 ˚C (red), and 280 ˚C

(blue). The mole ratio was 0.3:1 Pb:Zn, and the Pb precursor temperature was 150 ˚C at injection.

Notably, the intensity of the bandgap peak significantly decreased with respect to surface state peak in the doped trials. **Table 4.1** contains the quantitative peak ratios for **Figure 4.3**, showing that as the temperature increases, the peak at ~600 nm decreases relative to the peak at ~360 nm.

Table 4.1: Peak Ratios at Varying Zn Reaction Flask Temperatures

Zn Reaction Flask Temperature	Peak Ratio (~360 nm : ~600 nm)
200 °C	1 : 2
230 °C	1 : 1
280 °C	1 : 0.2

As a control, the fluorescence spectra of the doped trials were compared to those from mixtures of PbS NCs and ZnS NCs in **Figure 3.7b**. In all cases, the bandgap and surface state emission features are observed, and the addition of Pb decreases the overall fluorescence intensity. Additionally as seen in both the doped trials and the PbS and ZnS NCs mixture, the addition of Pb leads to changes in the relative intensities of the ~400 and ~600 nm peaks. Specifically, the surface state intensity increased relative to bandgap emission. The data in **Table 4.1** suggests that the ZnS NCs are much larger as

the heat increases. This would decrease the surface states peak at ~600 nm as the surface to volume ratio decreases.

However, there is a key difference between the spectra of mixed NCs and the spectra from doping trials—as seen in **Figure 4.3**, a shoulder near 715 nm appears in NCs from doping trials, and the relative intensity of this feature increases as the Zn flask temperature increases. At lower Zn reaction flask temperatures this feature appears as a shoulder on the much larger 600 nm peak. However, once the Zn flask temperature reaches about 280 °C, the peak at 715 nm is larger in intensity than the surface state emission. The shoulder at 715 nm clearly corresponds to the addition of Pb to the sample during synthesis, but the exact origin of this feature in unclear, as will be discussed in detail later.

TEM micrographs as a function of increasing Zn reaction flask temperature are shown in **Figure 4.4**. As expected, the ZnS NCs become larger as the Zn flask temperature increases. The observed size increase correlates well with the fluorescence data. As the ZnS NCs become larger the number of metal atoms in the bulk of the NC increases at a faster rate than the number of metal atoms on the NC surface. Therefore, when the NC size increases, the spectral affects coming from the surface atoms are expected to decrease relative to those coming from the bulk. This means that there would be a decrease in the peak at ~600 nm as the ZnS reaction flask temperature increases due to the decrease of available surface states. The TEM images clearly show

75

both ZnS NCs and PbS NCs in all doping trials, as shown in **Figure 4.5** below, while the

EDS data (not shown) confirms the presence of Pb, Zn, and S in all products.
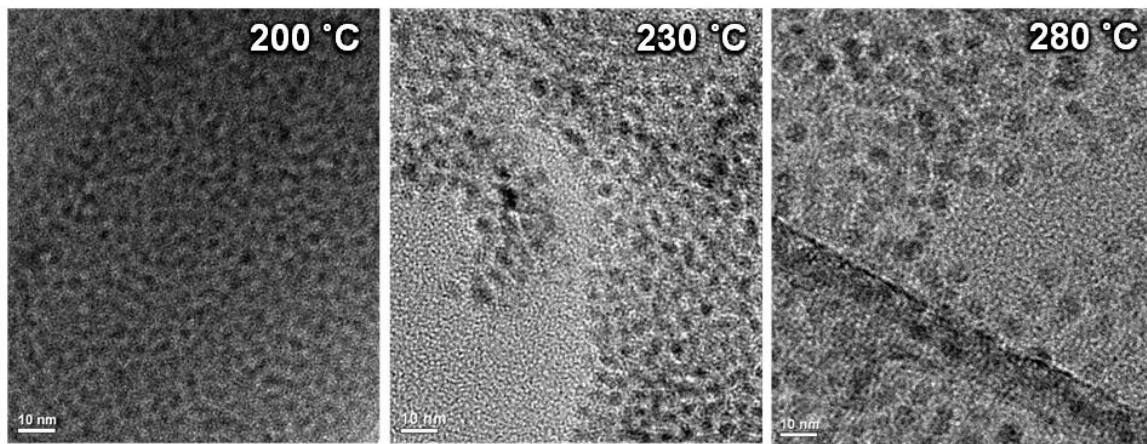
Figure 4.4: TEM images of product produced through doping trials with Zn reaction flask

temperatures of 200 °C (left), 230 °C (center), and 280 °C (right), all with a 10 nm scale

bar.
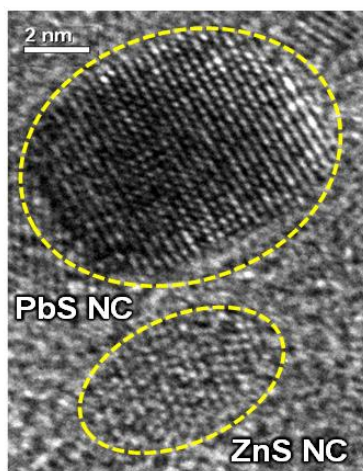
Figure 4.5: TEM images of typical product produced through doping trials. Image clearly

shows defined PbS and ZnS NCs

4.3 Variable 2: Pb Precursor Flask Temperature

As discussed previously, the temperature of the Pb precursor flask affects the precursor chemistry—when kept at room temperature, the Pb precursor is a mixture of PbO and oleylamine, while heating generates lead oleylamine complex prior to injection into the Zn reaction flask. When the Pb flask was kept at room temperature (20 °C), the purified products from the doping trials appeared as a grey/white cloudy colloids suspended in hexanes. When the Pb flask was heated to 150 °C, the purified products were dark brown/black colloids suspended in hexanes. Absorbance spectra as a function of Pb precursor temperature are shown in **Figure 4.6. Figures 4.6a-b** demonstrate the effects of Pb precursor flask temperature at mole ratio of 0.3:1, and a Zn reaction flask temperature of 230 °C and 280 °C respectively. These absorbance spectra are similar to the absorbance spectra of ZnS NCs in **Figure 3.5a**. Both absorbance spectra show a peak at ~310 nm. This peak corresponds to the electronic transition from VB to CB transition in ZnS NCs. The fine structure of this peak corresponds to the NCs' shape, size, and size distribution, which varies between samples. Also, in some cases there a feature appears near 900 nm; PbS NCs absorb in this region, as seen in **Figure 3.5b**. When the Pb flask was heated to 150 °C, the fluorescence spectra show the feature at ~610 nm as discussed above. The spectra from trials where the Pb precursor was kept at room temperature do not show the feature.

77
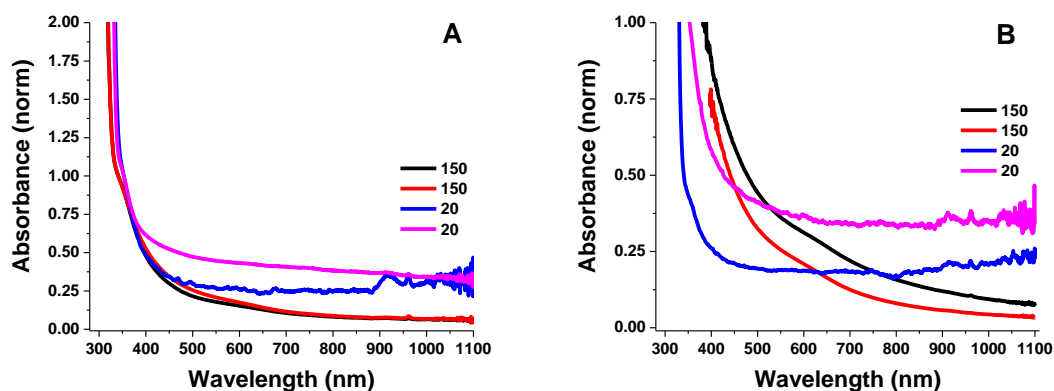
Figure 4.6: UV-Vis spectra of attempts at Pb-doped ZnS NC with the Pb flask temperature at 20 ˚C (blue and magenta) or 150 ˚C (black and red). Spectra (a) correspond to trials using a 230 °C Zn flask temperature, while spectra (b) correspond to a 280 °C Zn flask temperature. The Pb:Zn mole ratios was 0.3:1 in all cases.

The fluorescence spectra in **Figure 4.7** show clear differences in emission as a function of the Pb flask temperature prior to injection. **Figure 4.7** demonstrates the effects of Pb precursor flask temperature at mole ratio of 0.3:1 and a Zn reaction flask temperature of 280 °C. As discussed in the previous trials, the bandgap ZnS NC emission is seen at ~360 nm, the surface state emission near 600 nm is observed, the overall fluorescence intensity is decreased relative to that of ZnS NCs, and a shoulder at 715 nm is seen. Relative to the fluorescence spectra of ZnS NCs (**Figure 3.7a**), the surface state emission seen here is red shifted about 100 nm to 615 nm. The peak ratios for the ~360 nm, ~600 nm, and 715 nm peak are shown in **Table 4.2. Table 4.2** indicates that as the temperature of the Pb precursor flask increases from 20 °C to 150 °C, the ~600 nm peak

decreases relative to the ~360 nm peak, from a 1 : 0.40 (~360 nm : ~600nm) to a 1 : 0.13. The shoulder/peak present at 715 nm does not shift in energy with the changing Pb flask temperatures, but this feature is relatively more intense when the Pb is heated prior to injection. **Table 4.2** shows that as the temperature of the Pb precursor flask increases the 715 nm peak increases relative to the ~600 nm peak. The fact that pure PbS NCs do not fluoresce, and the lack of the 715 nm peak in the fluorescence spectra of the PbS/ZnS mixture as portrayed in **Figure 3.7b** both indicate that the doping products here are not simply mixtures of PbS NCs and ZnS NCs.
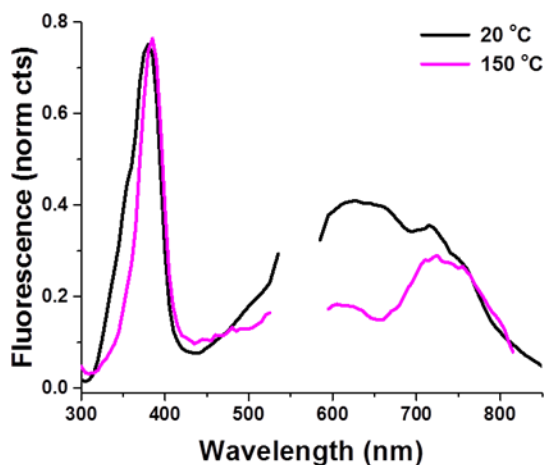
Figure 4.7: Fluorescence spectra of corresponding to attempts at Pb-doped ZnS NC for Pb flask temperatures of 20 ˚C (black) and 150 ˚C (pink). In all cases, a mole ratio of 0.3:1 Pb:Zn and a 280°C Zn flask temperature were used.

Table 4.2: Peak Ratios at Varying Pb Precursor Flask Temperatures

Pb Precursor Flask Temperature	Peak Ratio (~360 nm:~600 nm)	Peak Ratio (~600 nm:715 nm)
20 °C	1 : 0.40	1 : 0.92
150 °C	1 : 0.13	1 : 2.9

Because the peak at 715 nm increases as the Pb flask is heated to a higher temperature, it can be concluded that the chemical identity of the Pb precursor before injection can greatly affect the optical properties of the resulting NCs. When kept at room temperature, the PbO in the Pb flask does not form the lead oleylamine precursor complex prior to injection. This precursor complexation is thought to precede the Pb^{2+} monomer formation. Also, when the Pb flask is not heated past room temperature, the initial reagent PbO does not form precursor nor monomer before entering the Zn reaction flask. The result is that oxygen is added to the Zn flask while NCs are forming. This may lead to undesired oxidation of the NCs, though this was not investigated here.

TEM images of differing Pb precursor flask temperature trials are shown in **Figure 4.8**. When the Pb flask temperature is 20 ˚C, the PbS NCs in the product are larger those observed when the Pb flask temperature was 150 ˚C. This size difference may be due to the previously discussed differences in the Pb precursor injected. When the PbS NCs are smaller (Pb flask temperature prior to injection is 150 °C), there is a greater enhancement of the feature at ~715 nm as seen in the fluorescence data in **Figure 4.6** suggesting that this feature is related to the presence of Pb.
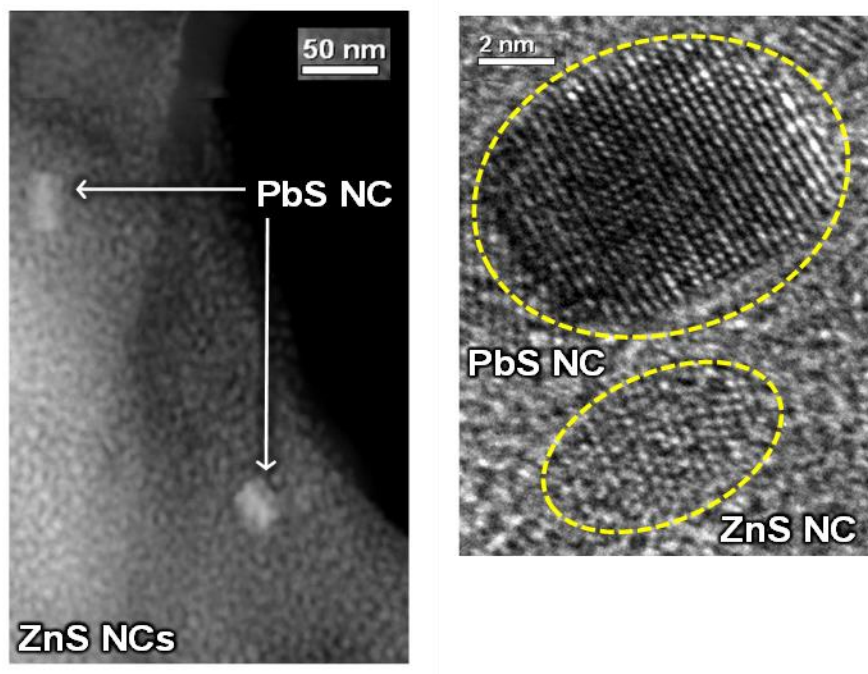
Figure 4.8: Images of product produced through doping trials with Pb flask temperature prior to injection of 20 ˚C (left, HAADF) and 150 °C (right, bright field TEM). Both samples were synthesized at 280 °C Zn flask temperature, and 0.3:1 Pb:Zn mole ratio. Note the difference in scales.

4.4 Variable 3: Changing Mole Ratio (Pb:Zn)

The UV-Vis absorbance spectra as a function of the Pb:Zn mole ratio are shown in **Figure 4.9. Figures 4.9a-c** demonstrate the effects of changing mole ratio (Pb:Zn) at a 150 °C Pb precursor flask temperature and a Zn reaction flask temperatures of 200 °C, 215 °C, and 230 °C respectively. All product produced during these trials appeared a dark brown/black color. The feature near 610 nm observed in all doping trials is seen in

these spectra, as well as the ZnS NCs feature at 360 nm, indicative of the VB to CB

absorbance of bulk ZnS NCs. The feature at 610 nm is much more pronounced at higher

Zn flask temperatures (**Figure 4.9c**) as well as higher Pb ratios (light blue and purple

lines).
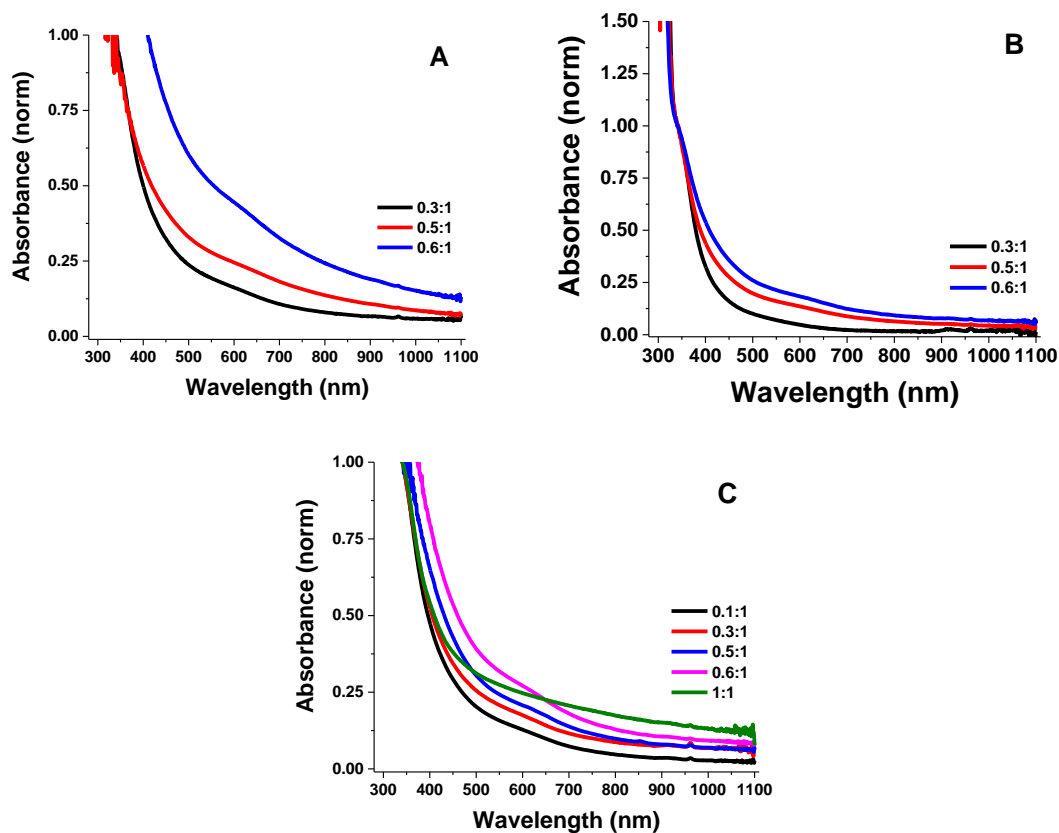
Figure 4.9: UV-Vis spectra of Pb-doped ZnS NC with changing mole ratio of Pb to Zn.

Spectra (a) correspond to a 200 °C Zn flask temperature, and a Pb flask temperature of

150 °C. Spectra (b) correspond to a 215 °C Zn flask temperature, and a Pb flask of 150 °C.

In spectra (a) and (b), the Pb:Zn mole ratios are 0.3:1 (black), 0.5:1 (red), and 0.6:1

(blue). Spectra (c) correspond to a 230 °C Zn flask temperature, and a Pb flask of 150 °C. In spectra (c) the Pb:Zn mole ratios are 0.1:1 (black), 0.3:1 (red), 0.5:1 (blue), 0.6:1 (magenta), and 1:1 (green)

Fluorescence spectra as a function of Pb:Zn mole ratio are shown in **Figure 4.10**. **Figure 4.10** demonstrates the effects of changing mole ratio (Pb:Zn) at a 150 °C Pb precursor flask temperature and a Zn reaction flask temperatures of 230 °C. The fluorescence spectrum in **Figure 4.10** is similar to that of ZnS NCs fluorescence spectrum in **Figure 3.7a**. Both show bandgap emission at ~360 nm and surface state emission at 600 nm. Relative to the fluorescence spectra of ZnS NCs, the peak at 515 nm was red shifted about 100 nm to 615 nm here. **Table 4.3** shows the peak ratios for the ~360 nm to ~600 nm. The most obvious trend seen in **Figure 4.10** is that with the addition of increased amounts of Pb there is a decrease in both the bulk ZnS NCs band gap peak (~300 nm), as well as the ZnS NCs surface states peak (~600 nm). The surface states peak decrease is much more pronounced than that of the bulk ZnS peak. This decrease in the surface states peak is due to the greater addition of Pb and the quenching effect it has on the ZnS surface states and bulk peaks. The PbS NCs are numerous and very large at higher mole ratios. This leads to an increased amount of quenching and less surface states do to the larger PbS NCs. The Pb to Zn mole ratio seems to have little to no impact on the presence or intensity of the ~710 nm as can in **Table 4.3**.

83
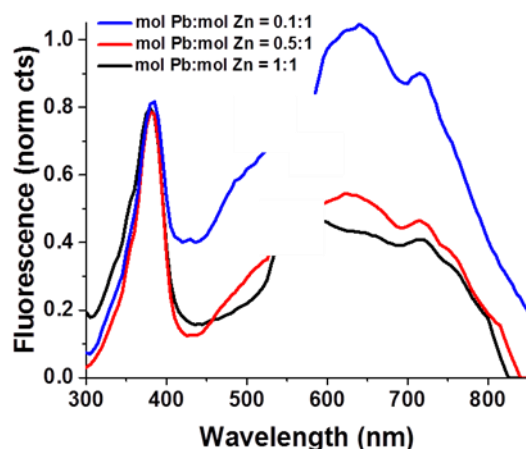
Figure 4.10: Fluorescence spectra of Pb-doped ZnS NC with changing mole ratio of Pb to Zn. Spectra is at a 230°C Zn flask temperature, and a Pb flask of 150°C. The Pb:Zn mole ratio, 0.1:1 (blue), 0.5:1 (red), and of 1:1 (black) are displayed.

Table 4.3: Peak Ratios at Varying Mole Ratios (Pb:Zn)

mol Pb:mol Zn	Peak Ratio (~360 nm:~600 nm)	Peak Ratio (~600 nm:715 nm)
0.1 : 1	1 : 1	1 : 0.88
0.5 : 1	1 : 0.54	1 : 0.87
1 : 1	1 : 0.45	1 : 0.95

TEM and HAADF images of the products at as the mole ratio of Pb:Zn increases are shown in **Figure 4.11**. As the Pb mole ratio increased the PbS NCs became more abundant and much larger. This makes sense; as the availability of Pb increases more PbS NCs and larger PbS NCs are can form. Incorporation of Pb into the ZnS would undoubtedly cause lattice strain, which may have prevented doping even at high Pb concentrations. As the size and number of PbS NCs increase, there is a decrease in the

relative surface state emission at ~600 nm, as seen in **Figure 4.9**. This seem rational

because as more Pb is added to a solution the overall fluorescence decreases as seen in

Figure 3.7b, which shows the fluorescence spectra of ZnS NCs as an increasing amount

of PbS NCs are added.
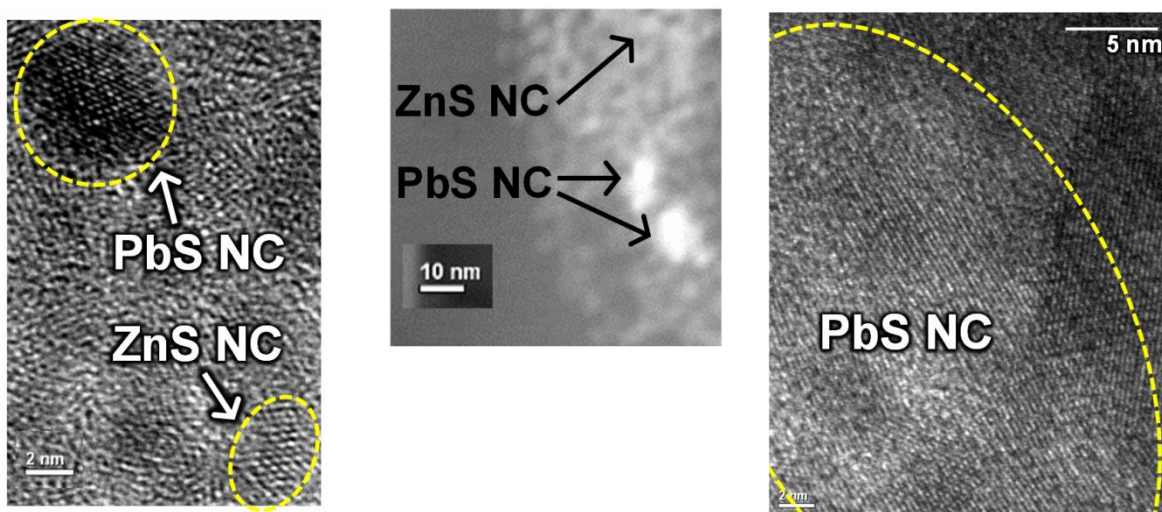
Figure 4.11: Images of product produced through doping trials with changing Pb:Zn

mole ratio. Left is a TEM image of 0.1:1 mole ratio of Pb:Zn, center is HAADF of the same

NCs, and right is a TEM image of a product from a 1:1 mole ratio of Pb:Zn. All images

were taken at 230 °C Zn flask temperature, and a 150 °C Pb flask temperature. Note the

difference in scales.

4.5 Summary of Results

The TEM and HAADF data clearly indicate the presence of a mixture of PbS NCs and ZnS NCs of various sizes and ratios. However, the optical properties of the NCs from doping trials do not completely match the optical properties of mixtures of PbS NCs and ZnS NCs. The UV-Vis spectra of the doped trials clearly show a feature present near 610 nm that is not present in the UV-Vis spectrum of a mixture of PbS NCs and ZnS NCs. More importantly though, the fluorescence spectra of the doped trials show a peak near 715 nm which is not observed in the fluorescence spectra of the mixture of PbS NCs and ZnS NCs.

The origins of this ~715 nm peak are still being debated among scientist, however, a 2006 paper by Kumar and Jakhmola provides a very insightful outlook on this particular peak in the fluorescence spectrum.[30] In their experiment Kumar and Jakhmola synthesized core-shell structures of PbS/ZnS and ZnS/PbS then measured the respective fluorescence activity. The nanoparticles were synthesized using an interfacial exchange of Zn^{2+} for Pb^{2+} from ZnS and vice versa. Some of these nanoparticles also showed a fluorescence peak at 680 – 715 nm. The authors claim that this fluorescence is the result of the formation of small, size-quantized PbS particles forming on the surface of the ZnS nanoparticles.[30] The ZnS NC fluorescence is quenched by the addition of Pb to the mixture due to a high density of trap states at the interface of the two NCs, PbS and ZnS, thus resulting in a fluorescence at 680 – 715 nm due to the electronic transitions between trap states [30] However, Kumar and Jakhmola's NCs also feature a hydroxide

interface between their PbS and ZnS NCs. The NCs synthesized in our work do not have such an interface.

In our work, the emission peak observed near 715 nm may be attributed to the formation of very small PbS NCs on the surface of the ZnS NCs. The Pb flask temperature had the highest impact on the intensity of the 715 nm peak. When the Pb flask temperature was higher, and thus smaller PbS NCs formed, there was a greater enhancement of the 715 nm feature. This data supports the hypothesis that small PbS NCs may have attached themselves to the surface of the ZnS NCs. An unlikely, but more desirable, outcome is that the ZnS NCs have been surface doped, meaning that one or two Pb atoms are incorporated into the surface layer of a ZnS NC. Doping at this level is likely not detectable with the available TEM. Future trials are needed to more definitively understand the atomic-level phenomena thought to be occurring. These future trials will be discussed in the following chapter.

CHAPTER 5

CONCLUSIONS AND FUTURE DIRECTIONS

5.1 Conclusions

The world is in need of an alternative energy source. There may be enough fossil fuels to sustain the world for the foreseeable future, but they are increasing expensive as they become more difficult to reach and are often located in politically and economically unstable places. Also the burning of fossil fuels releases GHGs into the atmosphere, which leads to a number of negative environmental consequences, including rising temperature, rising sea levels, and increasing ocean acidity.[3]

The research presented here addresses the need for an alternative energy source by developing a photocatalyst for H_2 *(g)* generation. H_2 *(g)* can be burned and used for fuel. As can be seen in **Figure 1.7**, the formation of Pb-doped ZnS NCs provides the photocatalyst with a sufficient CB for the reduction of H^+ *(aq)* to H_2 *(g),* as well as the ability to absorb a larger amount of solar photons from the sun. Pb-doped ZnS NCs are also made from cheap, earth abundant material which can help bring down the cost of alternative energy.

In all of the doping trials conducted here, mixtures of ZnS NCs and PbS NCs were produced. Generally, increased Zn flask reaction temperature leads to larger ZnS NC, as

evidenced by the TEM images as well as the fluorescence data, where there was decreased surface state emission relative to the bandgap emission, implying less surface area relative to the bulk of the NC. Increasing the Pb flask temperature, thus having Pb^{2+} monomer present before injection results in smaller PbS NC due to the increase in energy and lack of oxygen. Thus higher concentration of nucleation that occurs. Lastly, increased mole ratio of Pb to Zn leads to larger of larger PbS NCs.

The reactions conditions used during doping trials did generate different products with varied optical properties. The absorbance spectra from the doping trials show a feature at 610 nm that is not found in the spectra of mixtures of PbS NCs and ZnS NCs. The fluorescence spectra from the doping trials are closely resemble the fluorescence spectra of ZnS NC, with one notable exception—the peak at 715 nm. This peak is not observed in the PbS and ZnS NC mixture but it is present in the products from doping trials. This 715 nm peak is more prevalent at when the Pb precursor flask was elevated and smaller PbS NCs were observed in the TEM images. The origin(s) of this peak are unclear and debated in literature.[30–32] We hypothesize that this peak may arise from fused PbS NCs and ZnS NCs, energy and/or electron transfer between PbS NCs and ZnS NCs, or surface doping of the ZnS NCs with Pb ions. Further in depth instrumental analysis is needed to confirm these or other hypotheses.

5.2 Future Directions

Several types of characterization can be used to analyze future products from doping trials such as those described here. The absorbance and fluorescence data indicate that a material different than that of any controls was produced, as seen by the absorbance feature at 610 nm and the fluorescence feature at 715 nm. The TEM and EDS can provide a generic ratio of Pb to Zn present in the sample but cannot offer exact NC specifications, such as the position and chemical structure of each NC. X-ray diffraction (XRD) and photoelectron spectroscopy (PES) are two techniques that could yield a better understanding of the atoms comprising each NC.

XRD spectroscopy uses x-rays which are produced in the same was as an EDS, however in XRD the sample and detector rotate so that the x-rays produced are reflected at certain angles. This not only identifies the element, as in EDS, but also shows its placement within the NC structure. EDS measures the intensity of an X-ray that results from electrons hitting certain atoms. Each X-ray intensity is indicative of a certain element. However, XRD also measures the angle at which the X-ray enters the detector, then as the sample rotates the detector can collect X-rays from all sides of the NCs and create a diffraction pattern corresponding to the crystal structure of the NC.

Photoelectron spectroscopy can also identify elements present in the sample, provide information on the chemical environment(s), and yield the density of states in the valence band of the sample. In this technique an x-ray or ultraviolet source ejects electrons from the core or valence orbitals of the atom respectively. Then, the kinetic

energy (KE) of the ejected electron after it leaves the sample surface is measured. This kinetic energy reflects the binding energy (BE) of the electron—high KE electrons were loosely bound (low BE), while low KE electrons originate from tightly bound environments (high BE). Kinetic energy of the ejected electron is used to calculate the binding energy that was keeping the electron attached to the atom, and the binding energy is specific for each element due to its specific number of protons. We would expect electrons from Pb in PbS NCs to have different KE than electrons from Pb atoms doped into ZnS NCs. Additionally, we would expect the density of states generated for Pb-doped ZnS NCs to differ from those of pure ZnS NCs or pure PbS NCs.

There are also a few options for altering the synthetic strategy to achieve doping. One would be to expand the mole ratio between Pb and Zn. In this project a 0.1:1 to 1:1 mole ratio of Pb to Zn was used, however it may be helpful to expand that ratio. Decreasing the Pb concentration even further, to maybe 0.05:1, may still produce Pb-doped ZnS NC. By decreasing the Pb concentration that decreases the chance the PbS NC can form because doping requires one or two Pb atoms per ZnS NC and this may be more difficult to achieve with lower Pb ratios.

Another synthetic strategy that could yield Pb-doped ZnS NCs is changing the length of the ligand/coordinating solvent used. By changing the length of the ligands present in the Zn precursors and the Pb precursors, one can systematically vary the relative reactivity of the Pb and Zn precursors. The activity of the precursor is effected by the bonding strength of the coordinating solvent and it's steric effects.[33] Increasing

91

the chain length of the coordinating solvent increases the reactivity of the Pb and Zn precursor and thus decreases the size of the overall NC.[34] Future students, who work on this project, may find that by increasing or decreasing the chain length of the coordinating solvent may allow the Pb and Zn precursor the appropriate energy to form doped NC. Trying such chain lengths as those suggested in **Table 5.1** may be interesting. The current coordinating solvent is oleylamine, which has a chemical formula of $C_{18}H_{37}N$.

Table 5.1: Suggested Coordinating Solvents for Synthesis

Chemical Name	Chemical Formula
Dodecylamine	$C_{12}H_{27}N$
Tetradecylamine	$C_{14}H_{31}N$
Hexadecylamine	$C_{16}H_{35}N$
Octadecylamine	$C_{18}H_{39}N$

Post synthetic doping strategies may also be employed for the successful synthesis of Pb-doped ZnS NC. This involves the synthesis and purification of ZnS NC and then heating the sample with the addition of Pb^{2+} ions. The driving force for any cation exchange reaction is the net thermodynamic force (energies of formation), lattice energy, as well as the ligand environment present, which may alter the reduction potential of the NC.[35] Post synthetic doping has been seen with many binary NC systems and may be found effective here as well.

Once Pb-doped ZnS NCs are successfully and reproducibly synthesized and characterized, then the photocatalytic ability of the NCs for generation H_2 *(g)* can be

measured. The reduction of hydrogen ions to form H_2 *(g)* is hard to detect and quantify because the hydrogen is gaseous, clear and colorless. One way to qualitatively determine the NCs ability to reduce protons is to employ another compound with a reduction potential near that of hydrogen ions. This other compound should also have some kind of physical change to indicate that the reduction has taken place. The compound that will be used for this experiment is methyl viologen. Methyl viologen has two oxidation states that exhibit two different colors. The 2+ state of methyl viologen is colorless , and the 1+ state is deep blue in color.[36] Once an electron from the doped NC is photoexcited, an electron transfer from the NC to the viologen cation can occur if the excited electron has enough energy to reduce methyl viologen. This electron transfer event will be accompanied a color change, and the color change can be monitored using a UV-Vis absorbance spectroscopy. The reduction potential of methyl viologen is -0.446 V for the 2+ to 1+ state against the standard hydrogen electrode.[37] When a color change is observed, the researcher will know that the CB energy of their NC has a significant energy to reduce H^+ *(aq)* to H_2 *(g).*

5.3 Outlook

Once realized, Pb-doped ZnS NCs may be used to absorb a large amount of solar photons, then convert those solar photons into electrons that form bonds between hydrogen ions from water to finally yield H_2 *(g)*, which can be stored and used when the sun is not out. These NCs will have a high surface area, are made from cheap, earth-

abundant materials, absorb a large portion of the solar emission spectra, and have a CB sufficient enough to produce H_2 *(g)*. This new energy collection method could reduce the dependence on oil and natural gas, as well as reduce the GHGs released into the atmosphere. Also this new energy collection method is renewable, as the result of burning H_2 *(g)* for energy is the production of water, which can be recycled to the beginning of the process. Ultimately, this work is an example of the ways in which fundamental science can be understood and manipulated to generate much-needed functional materials for energy conversion, generation, and storage.

LIST OF REFERENCES

(1)   Cook, T. R.; Dogutan, D. K.; Reece, S. Y.; Surendranath, Y.; Teets, T. S.; Nocera, D. G. *Chem. Rev.* **2010**, *110*, 6474–6502.

(2)   How much coal, natural gas, or petroleum is used to generate a kilowatthour of electricity? https://www.eia.gov/tools/faqs/faq.cfm?id=667&t=2 (accessed Jan 2, 2016).

(3)   Marquis, M.; Tans, P. In *Fundamentals of Materials for Energy and Environmental Sustainability*; Ginley, D. S.; Cahen, D., Eds.; Cambridge University Press, 2011; pp. 1–24.

(4)   Molecular Vibrations http://www2.ess.ucla.edu/~schauble/molecular_vibrations

.htm (accessed Mar 1, 2016).

(5)   Archer, D.; Eby, M.; Brovkin, V.; Ridgewell, A.; Cao, L.; Mikolajewicz, U.; Caldeira, K.; Matsumoto, K.; Munhoven, G.; Montenegro, A.; Tokos, K. *Annu. Rev. Earth Planet. Sci.* **2009**, *37*, 117–134.

(6)   Lewis, N. S. *MRS Bull.* **2007**, *32*, 803–820.

(7)   Solar Panel Efficiency http://pureenergies.com/us/how-solar-works/solar-panel-efficiency/ (accessed Feb 1, 2016).

(8)   Kamat, P. Photocatalysis https://www3.nd.edu/~kamatlab/research_photo catalysis.html (accessed Mar 1, 2016).

(9)   Chakrapani, V.; Baker, D.; Kamat, P. *J. Am. Chem. Soc.* **2011**, *133*, 9607–9615.

(10)   Hydrogen Info http://basicsofhydrogen.weebly.com/hydrogen-info.html (accessed Feb 1, 2016).

(11)   International Standard - Switzerland http://www.iec.ch/ (accessed Feb 1, 2016).

(12)   Osterloh, F. E. *Chem. Soc. Rev.* **2013**, *42*, 2294–2320.

(13)   Tsuji, I.; Kudo, A. *J. Photochem. Photobiol. A Chem.* **2003**, *156*, 249–252.

(14)   Perraut, D. Synthesis anf Characterization of Pb2+ - Doped ZnS Nanocrystals for Photocatalyzed Hydrogen Gas Generation, Eastern Kentucky University, 2015.

(15) Carey, G.; Abdelhady, A.; Ning, Z.; Thon, S.; Bakr, O.; Sargent, E. *Chem. Rev.* **2015**, *115*, 12732–12763.

(16) Hines, M. a.; Scholes, G. D. *Adv. Mater.* **2003**, *15*, 1844–1849.

(17) Cass, L. C.; Malicki, M.; Weiss, E. a. *Anal. Chem.* **2013**, *85*, 6974–6979.

(18) Zhai, X.; Zhang, X.; Chen, S.; Yang, W.; Zheng, G. *Colloids Surfaces A Physicochem. Eng. Asp.* **2012**, *409*, 126–129.

(19) Weiss, E. A. *Acc. Chem. Res.* **2013**, *46*, 2607–2615.

(20) Thomson, J. W.; Nagashima, K.; Macdonald, P. M.; Ozin, G. a. *J. Am. Chem. Soc.* **2011**, *133*, 5036–5041.

(21) No Title http://bilbo.chm.uri.edu/CHM401/fall2011exam2-1.html (accessed Apr 19, 2016).

(22) Chapter 7: The Crystalline Solid State http://www.chem.uci.edu/~lawm/Ch 7 Solutions.pdf.

(23) Thanh, N. T. K.; Maclean, N.; Mahiddine, S. *Chem. Rev.* **2014**, *114*, 7610–7630.

(24) Clark, M. D. *J. Nanoparticle Res.* **2014**, *16*, 2264.

(25) Viswanatha, R.; Sarma, D. D. *Nanomater. Chem.* **2007**, 139–170.

(26) van Embden, J.; Chesman, A. S. R.; Jasieniak, J. J. *Chem. Mater.* **2015**, *27*, 2246–2285.

(27) University, M. S. UV Visible Absorption Spectroscopy http://faculty.sdmiramar.edu/fgarces/LabMatters/Instruments/UV_Vis/Cary50.htm#Theory. (accessed Mar 1, 2016)

(28) Basic Principle of Transmission Electron Microscope http://www.hk-phy.org/atomic_world/tem/tem02_e.html. (accessed Mar 1, 2016).

(29) Pichaandi, J.; van Veggel, F. C. J. . *Coord. Chem. Rev.* **2014**, *263*, 138–150.

(30) Kumar, A.; Jakhmola, A. *J. Colloid Interface Sci.* **2006**, *297*, 607–617.

(31) Kumar, A.; Jakhmola, A.; Chaudhary, V. *J. Photochem. Photobiol. A Chem.* **2009**, *208*, 195–202.

(32)   Kim, J.; Kim, S. G.; Oh, E.; Kim, S. H.; Choi, W. J. *Nanotechnology* **2016**, *27*, 1–6.

(33)   Yu, W. W.; Wang, Y. A.; Peng, X. *Chem. Mater.* **2003**, *15*, 4300–4308.

(34)   De Nolf, K.; Capek, R. K.; Abe, S.; Sluydts, M.; Jang, Y.; Martins, J.; Cottenier, S.; Lifshitz, E.; Hens, Z. *J. Am. Chem. Soc.* **2015**, *137*, 2495–2505.

(35)   Beberwyck, B. J. Cation Exchange Reactions for Improved Quality and Diversity of Semiconductor Nanocrystals, Univerisrt of California, Berkeley, 2014.

(36)   Maruszewski, K.; Hreniak, A.; Czyzewski, J.; Wieslaw, S. *Opt. Mater. (Amst).* **2003**, *22*, 221–225.

0(37)   Kim, S. M.; Jang, J. H.; Kim, K. K.; Park, H. K.; Bae, J. J.; Yu, W. J.; Lee, I. H.; Kim, G.; Loc, D. D.; Kim, U. J.; Lee, E.-H.; Shin, H.-J.; Choi, J.-Y.; Lee, Y. H. *J. Am. Chem. Soc.* **2009**, *131*, 327–331.